NORTHWESTERN UNIVERSITY

Graph Theoretical Insights into Structural and Functional Network Architecture Underlying Bipolar Spectrum Disorders

A DISSERTATION

SUBMITTED TO THE GRADUATE SCHOOL

IN PARTIAL FULFILLMENT OF THE REQUIREMENTS

for the degree

DOCTOR OF PHILOSOPHY

Field of Psychology

By

Katherine S. F. Damme

EVANSTON, ILLINOIS

September 2018

Abstract

Individuals at high-risk for and with a bipolar spectrum disorder (BSD) show emotion regulation network abnormalities compared to low risk individuals. BSDs are characterized by emotion dysregulation at varying levels of severity. Frequently, individuals with a less severe BSD diagnosis frequently advance to a more severe diagnosis over time. Based on this tendency, early detection may be particularly critical for individuals on the bipolar spectrum. Previous research on BSD compares healthy individuals to severe forms of bipolar disorder. Although this approach is unable to dissociate correlates of vulnerability to BSD from correlates of BSD. To address this first gap in the literature, the present study compared individuals along a spectrum of risk to dissociate correlates of vulnerability for BSD from correlates of BSD. One critical risk marker of BSD may be the architecture of neural networks, particularly those networks involved in reward and emotion. However, no study has examined structural and functional network architecture of BSD along a spectrum of risk. To address this second gap in the literature, these analyses used a graph theoretical approach to examine both structural (diffusion tensor) and functional (resting-state) network architecture implicated in BSD across three network definitions: a) whole brain network composition, b) theoretically defined emotion generation/regulation subnetwork, and c) theoretically defined reward subnetwork. Within each of these network definitions, graph metrics were calculated as global metrics, nodal metrics, and theoretical internetwork hub regions. Risk for BSD related to decreased structural and functional network efficiency in emotion regulation regions.

Acknowledgements

"If I have seen further, it is by standing upon the shoulders of giants" - Sir Isaac Newton

My ideas never develop in the dark; I am forever in debt to those who helped rough ideas blossom. My deep gratitude first goes to my masters and doctoral committee members: Robin Nusslock, Paul Reber, and Vijay Mittal. My appreciation also goes to my laboratory colleagues, especially, Nicholas J. Kelley my reader/editor on everything. I am also grateful for my numerous training opportunities, including my ThinkSwiss fellowship, NIMH IRTA fellowship, Neurobiology of Information Storage fellowship, and Human Cognition fellowship. Prior to graduate study, I received unparalleled mentorship and continued support from amazing scientists. In particular thanks to David Zald for mentoring me through my awkward early years of science and continuing to be a role model, mentor, and friend. While I've learned a great deal from those who dedicated their time to training me, I've also learned a great deal from those that I have had the opportunity to train: Rita Taylor, Virginia Hoch, Ajay Nadig, Laura Padilla, Wan Kwok, and Michael Weston, thank you for everything. Finally, I would like to thank my family their patience, support, and encouragement. The long hours spent working toward this degree were, in fact, long hours spent away from my family. I truly could not have done any of this without your support and patience.

Dedication

To My Husband Tyler Damme

You've sacrificed as much as I have for my PhD. Thank you for moving around the country for me. Thank you for always having confidence in my abilities when I doubted myself. Thank you for always being understanding when the time demands of a PhD overwhelmed our shared life. Thank you for all the late nights that you slowly closed my laptop on my hands because it was time for bed. Thank you for being a shoulder to cry on when I was too tired to sleep. Thank you for the early mornings that you drove me to campus. Thank you for covering everything that I was too busy to do over the past five years. We are very different from the teenagers that fell in love thirteen years ago, but one thing is always the same; you have always been supportive and helped me make my dreams come true. You were, you are, and you always will be my best friend and the love of my life. There is no way I could have done this without you.

Table of Contents

List of Tables

List of Figures

Introduction

Bipolar spectrum disorders (BSD) are debilitating illnesses that affect approximately 4.4% of the global population (Angst, Stassen, Clayton, & Angst, 2002; Merikangas et al., 2007). All BSD diagnoses are defined by emotion dysregulation, including extreme highs (hypo/mania) and lows (depression) that impact mood, motivation, cognition, and behavior (Nusslock & Alloy, 2017). BSD diagnoses include several subtypes: cyclothymia, bipolar II disorder, and bipolar I disorder (Alloy et al., 2012a; Alloy et al., 2012b; Birmaher et al., 2009; Cassano et al., 1999). The primary distinguishing feature between each subtype is severity, with cyclothymia the least severe and bipolar I disorder being the most severe (Nusslock & Alloy, 2017). Frequently, less severe BSD diagnoses progress in symptom severity, meaning individuals with milder forms of bipolar disorder (e.g., cyclothymia, bipolar II) are more likely to develop bipolar I disorder in the future (Alloy et al., 2012a; Alloy et al., 2012b; Birmaher et al., 2009; Kochman et al., 2005). This tendency for BSD to progress in symptom severity highlights the importance of early corollaries of vulnerability that may aid in early intervention and prevent disease progression (Angst, Stassen, Clayton, and Angst, 2002; Cassano et al., 1999). The literature to date, however, has not dissociated correlates of vulnerability to BSD from correlates of BSD. As a result, neural mechanisms related to vulnerability for BSD remain poorly understood.

High-risk designs are a useful methodological approach to dissociate correlates of vulnerability from the correlates of the presence or progression of BSD. Unfortunately, research on BSD has typically not examined high-risk populations, but instead has compared healthy individuals to individuals with a BSD. While comparing healthy controls to BSD has identified critical abnormalities associated with BSDs, this approach leaves ambiguity as to whether

observed abnormalities are correlates of vulnerability to BSD or correlates of the presence and progression of BSD (see Alloy & Nusslock, 2018; Nusslock, Young & Damme, 2014). Examining BSD in a high-risk design may help dissociate whether an abnormality is a correlate of risk or correlate of BSD. Early markers of vulnerability, or correlates of risk, should appear in individuals at high-risk for BSD and in individuals with BSD diagnoses, but not in healthy control individuals. In contrast, correlates of the presence or progression of a BSD should only appear in the BSD group, and should not appear in high-risk or healthy populations. Therefore, high-risk designs provide a critical window into the pathophysiology of BSD.

Previous BSD studies leave room for methodological innovations in key ways (see Nusslock, Young, & Damme, 2014 for a review). First, many studies of BSD focus on brain structure and function in a small set of neural regions. This approach overlooks the importance of connections between regions. For example, elevated activation in one region could be driven by increased excitatory connectivity to that region, decreased inhibitory connectivity to the region, or connections within the region itself. Therefore, examining regional changes in isolation of their neural network provides limited insight into the mechanisms underlying elevated activation. As a result, questions remain as to whether a particular region itself is aberrant, or if activity in that region is a downstream effect of an abnormal network. Second, BSD literature examining connectivity typically focuses on only a small set of pairwise connections, which provides limited insight into the network features. Both regional and connectivity approaches presume the presence of a largely intact network structure with key disruptions between limited regions and overlooks the possibility that BSD is related to a broad restructuring of network architecture. Finally, past work examining structural connectivity has been largely limited to examining direct

anatomical connections between two regions (e.g., medial orbitofrontal cortex to nucleus accumbens), or large, non-specific white matter tracts (e.g., uncinate fasciculus). These structural connectivity approaches are unable to characterize distant structures that are indirectly connected in a larger network (e.g., pathways from dorsal portions of the prefrontal cortex PFC to the nucleus accumbens via the orbitofrontal cortex). These long-range connections may be critical to the overall function of the network and relevant to understanding psychiatric illness. In summary, current regional and pairwise connectivity approaches provide incomplete insight into neural networks. As a result, there is uncertainty as to whether BSD abnormalities may be driven by network architecture, connections between neural regions, or specific areas of the brain.

Graph theory analyses can address these methodological limitations by quantifying key network organizational properties. Critically, graph theory metrics allow each brain region to be examined in terms of its larger network context, by quantifying connections between multiple regions that are directly or indirectly connected. To date, only a handful of studies have examined BSD using graph theory analyses on structural (i.e., diffusion tensor imaging; Collin et al., 2016; GadElkarim et al., 2014; Leow et al., 2013) or functional data (Manelis et al., 2016; Roberts et al., 2017; Spielberg et al., 2016). Presently, no BSD studies have used behavioral high-risk design in conjunction with graph theory analyses (although see Roberts et al., 2017 for genetic high-risk design). Furthermore, past studies examine network properties of single regions (Collin et al., 2016; GadElkarim et al., 2014; Roberts et al., 2017) or exploratory whole brain network properties (Collin et al., 2016; GadElkarim et al., 2014; Leow et al., 2013; Manelis et al., 2016; Spielberg et al., 2016); this approach fails to examine subnetwork properties established in theoretical neurobiological models of BSD.

Current neurobiological literature of BSD focuses on two major theoretical models: the emotion regulation model and the reward hypersensitivity model (Alloy & Nusslock, 2018; Marchand et al., 2011; Mayberg, 1997; Phillips, Ladouceur, & Drevets, 2008; Strakowski et al., 2012). The emotion regulation models focus on interactions between emotion generation and emotion regulation in a broader emotion network. The emotional response or generation subnetworks are sensitive to emotionally relevant stimuli and drive emotional reactivity, while the emotion regulation subnetworks modulate emotional generation based on the context (Nusslock et al., 2012; Nusslock, Young, & Damme, 2014; Phillips, Ladouceur, & Drevets, 2008). Emotion regulation models tend to focus on affective dysregulation, and not on the predictive insight of reward sensitivity. In contrast, the reward hypersensitivity model highlights that reward sensitivity and reactivity to rewarding stimulus is predictive of hypo/mania. While this model has provided critical insight into BSD, it has primarily focused on the sensitivity to reward stimuli in BSD in a smaller number of neural regions. Though these models have distinct emphases, these models describe overlapping neural subnetwork regions that generate or regulate emotional responses. Disruptions in these subnetworks may underlie emotional dysregulation in BSD (Phillips, Ladouceur, & Drevets, 2008; Strakowski et al., 2012). These subnetworks have not been directly examined in network models of BSD. Instead these theories draw on studies of regional and pairwise findings to form network hypotheses. While regional and pairwise connectivity has provided evidence of abnormalities in BSD networks, they do not examine these networks as a whole.

Examining both emotion regulation and reward theoretical models may provide unique insight into features of BSD. Given that BSD is associated with significant emotion

dysregulation, abnormalities in emotion generation/regulation subnetwork may be correlates of BSD. Given that the reward hypersensitivity model is predictive of future BSD risk, reward network abnormalities may be particularly sensitive to corollaries of risk for BSD. Based on past literature, restricting graph network definitions from a whole brain network definition to a theoretically defined subnetwork may increase sensitivity to BSD differences (GadElkarim et al., 2014; Manelis et al., 2016; Wang et al., 2018). Similarly, restricting analyses from the larger emotion generation/regulation subnetwork to the smaller reward network may further increase sensitivity to BSD network abnormalities. Therefore, examining both theoretical subnetwork models may provide unique insights into correlates of risk or correlates of BSD. Additionally, both the emotion generation/regulation and reward models also identify critical hub regions in the brain that facilitate interactions between the emotion generation and the emotion regulation subnetworks (Phillips, Ladouceur, & Drevets, 2008; Strakowski et al., 2012). Disruptions in these subnetworks or critical hubs may underlie emotional dysregulation in BSD (Phillips, Ladouceur, & Drevets, 2008; Strakowski et al., 2012). As a result, these critical nodes will be examined in terms of whole brain network, emotional generation/regulation subnetwork and reward subnetwork connectivity as theoretical internetwork hubs.

Individuals at high-risk for and with a bipolar spectrum disorder (BSD) show emotion regulation network abnormalities compared to low risk individuals. To examine these networks as a whole, current study is the first to use a behavioral high-risk design to examine whether behavioral low-risk, behavioral high-risk, and BSD groups differ in structural or functional network architecture. Additionally, this is the first study to directly examine neurobiological theories of BSD in a network model. The present study used a behavioral high-risk model to

examine structural (Aim 1) and functional (Aim 2) network architectures at three network definitions: (a) whole brain, (b) emotion generation/regulation subnetwork, and (c) reward subnetwork. These networks were examined in terms of global graph metrics, nodal graph metrics, and theoretical inter-network hubs. While global metrics provide a broad overview of neural networks, they lack the specificity to directly test theoretically relevant regions, nodal metrics provide direct comparisons of brain region inside a given network. Whole brain network analyses compared overall structure, as well as critical global and nodal metrics (i.e., clustering coefficient, path length, and small world property). The subnetwork analyses were drawn from emotional generation/regulation and reward sensitivity literature to examine critical BSD subnetworks to increase specificity of structural metrics (i.e., clustering coefficient and path length) connections that are theoretically relevant to BSD. Finally, it is also possible that critical regions responsible for integrating input from both emotion regulation and emotion generation (internetwork hub regions) are also critical sites of abnormalities in BSD. Therefore, I have also examined theoretically informed hub regions identified as critical sites of integration between emotion generation and regulation.

In the following sections of the introduction, I begin by defining the behavioral high-risk model of BSD using the reward hypersensitivity model. Then, I provide an overview of graph theoretical analyses and discuss potential advantages this method provides in testing neurobiological models of BSD. Next, I review neurobiological models of BSD (the emotion regulation reward and hypersensitivity model) and define emotion generation, emotion regulation, and reward subnetworks. Finally, I discuss hypotheses regarding these theoretical subnetwork structure in a graph theory analytic approach.

Behavioral High-Risk Design

Past literature has compared healthy individuals to the most severe forms of BSD (i.e., bipolar I and bipolar II). While this has provided insight into features characteristic of BSD, it has been unable to determine if these features are correlates of risk or if they are correlates of the presence and progression of BSD. To separate correlates of risk from correlates of BSD, graph theory neural networks were compared across three groups in a behavioral high-risk model. These groups include a low risk for BSD group, a high risk for BSD group, and a BSD diagnoses group. Risk for BSD was defined behaviorally based on the reward hypersensitivity model. The reward hypersensitivity model has demonstrated that reward sensitivity is a reliable predictor of future BSD onset and course (Alloy et al., 2008). In the following section, I introduce the Reward Hypersensitivity Model of bipolar disorder and provide evidence that this model is predictive of future onset of a BSD (relating to risk for BSD) and relevant to BSD features across severity (relating to BSD course). I, then, describe the application of this high-risk model in the current study.

Reward Hypersensitivity Model of BSD Introduction. The reward hypersensitivity model proposes that individuals at high-risk for a BSD exhibit trait-like elevated reactivity to reward-relevant stimuli (Alloy, Nusslock, & Boland, 2015; Johnson, Edge, Holmes, & Carver, 2012; Urosevic, Abramson, Harmon-Jones, & Alloy, 2008). Additionally, the reward hypersensitivity model proposes that reward hypersensitivity is a central mechanism underlying BSD for several reasons. First, the model first proposed that hypo/mania is driven by a hypersensitivity to cues of possible reward (Alloy, Nusslock, & Boland, 2015; Johnson, Edge, Holmes, & Carver, 2012; Nusslock, et al., 2014; Nusslock, Young, & Damme, 2014). Second, individuals with BSD

experience an excessive increase in motivation during life events involving the pursuit or attainment of reward (Björn Meyer, Beevers, & Johnson, 2004). Finally, in the extreme, increased motivation is reflected in hypo/manic symptoms such as elevated mood, decreased need for sleep, and increased goal-directed activity. Thus, the reward hypersensitivity model argues that symptoms of hypo/mania involve extreme emotional reactivity along a core brain-behavior dimension of positive valence, reward-processing and incentive motivation.

Predictive Validity of the Reward Hypersensitivity Model. A large body of literature supports reward hypersensitivity as a trait that precedes onset of BSD (Alloy & Nusslock, 2018; Nusslock, Young, & Damme, 2014 for review). Both prospective and retrospective studies demonstrate that reward sensitivity is predictive of BSD onset and progression (Alloy et al., 2006; Alloy et al., 2008; Alloy et al., 2012a). In prospective studies, elevated self-reported reward sensitivity was associated with a greater likelihood of having a bipolar spectrum episode in the future (Alloy et al., 2012b). In fact, Alloy et al. (2012) demonstrated that reward sensitivity participants had significantly greater likelihood of developing a first onset of BSD (12.3%) compared to moderate reward sensitivity participants (4.2%) over a prospective one-year follow-up. This behavioral high-risk model has a similar, albeit slightly higher, conversion rate to the lifetime conversion rate of first degree relatives of BSD patients (9%; for a review see Barnett & Smolder, 2009). In retrospective and concurrent studies, individuals with elevated self-reported reward sensitivity were six times more likely to obtain a lifetime diagnosis of a BSD than were individuals with moderate reward sensitivity (Alloy et al., 2012b). Taken together these studies provide evidence that reward sensitivity is a predictive correlate of risk for BSD.

Reward Hypersensitivity across the Bipolar Spectrum. Reward sensitivity is observed across all levels of bipolar severity. Along a clinical dimension, individuals with either bipolar I disorder (Meyer, Johnson, & Winters, 2001), bipolar II disorder, or cyclothymia (Alloy et al., 2008) self-report higher levels of reward sensitivity than healthy controls. Reward hypersensitivity is also a valuable prospective predictor of the clinical course of BSD. For individuals with milder forms of BSD (e.g., cyclothymia) higher reward sensitivity is associated with a greater likelihood of progressing to more severe bipolar diagnoses (e.g., bipolar disorder I; Alloy et al., 2012a; Alloy et al., 2012b). Furthermore, recovered individuals with bipolar I disorder who have elevated reward sensitivity experience increases in manic symptoms (Meyer, Johnson, & Winters, 2001). Across all forms of BSD, elevated reward sensitivity is related to shorter time between manic episodes among individuals with BSD (Alloy et al., 2008). Taken together, this literature demonstrates that reward hypersensitivity is predictive of both initial onset and BSD progression at the level of symptom severity. Thus, across all levels of severity, reward hypersensitivity has been associated with BSD.

Reward Sensitivity Behavioral High-Risk Group Summary. Collectively, this work suggests that reward hypersensitivity is a predictive correlate of risk prior to BSD onset and a correlate of BSD onset and progression after BSD onset. Drawing on the reward hypersensitivity model, this project used a high-risk design that includes three groups: behavioral low-risk, behavioral high-risk, and BSD groups. Unlike past literature, which has largely compared individuals with or without a BSD, this high-risk design will allow us to distinguish correlates of risk from correlates of BSD. The definition and contribution of each risk group is described in the following section.

The behavioral low-risk group includes individuals with a moderate trait level of reward sensitivity (Low-Risk). The Low-Risk group is defined by moderate reward sensitivity for two reasons. First, moderate reward sensitivity is most typical in the population, thus, representing the most common trait level of reward sensitivity. Second, individuals with low levels of reward sensitivity have elevated risk for depression (Whitton, Treadway, & Pizzagalli, 2015 for review). As such, low reward sensitivity is, in fact, a high-risk group for depression and a biased control group. Therefore, the moderate reward sensitivity group represents the most typical and least clinically biased control sample. Accordingly, the Low-Risk was defined as moderate levels of reward sensitivity in the behavioral high-risk design.

The behavioral high-risk group includes individuals with high trait levels of reward sensitivity and no lifetime BSD diagnosis (High-Risk). High-risk is defined as high trait levels of reward sensitivity because, as previously discussed, this trait is highly predictive of future development of a BSD (Alloy et al., 2012a; Alloy et al., 2012b). Therefore, the High-Risk group was selected to have a similar level of reward sensitivity as the BSD group. Similar levels of reward sensitivity in the BSD and High-Risk groups ensured that the difference between groups could be attributed to the presence of a BSD diagnosis and not trait variability. Furthermore, in this design any differences between the Low-Risk group and the High-Risk group could be attributed to the increased behavioral risk for developing BSD. As a result, the addition of a behavioral High-Risk group aids in dissociating correlates of vulnerability to BSD from corollaries of BSD.

Finally, this high-risk design included a BSD group that was made up of individuals with any BSD diagnosis including BSD-NOS, cyclothymia, bipolar II disorder, and bipolar I disorder

(BSD). The BSD group included the full range of symptom severity, which increases the generalizability of the findings to all BSD diagnoses. Within the BSD group, all individuals had high reward sensitivity and did not significantly differ from the High-Risk group in terms of behavioral risk traits. As a result, any group differences between the High-Risk and BSD group may be attributed to the presence of a BSD diagnosis. Therefore, the BSD group is comprised of individuals with high reward sensitivity and a BSD diagnoses.

By comparing these three groups, the behavioral high-risk design can identify correlates of vulnerability to BSD by identifying network architecture that is common to BSD and High-Risk groups, but distinct from the Low-Risk group. Additionally, this approach may identify the distinct correlates of the presence or progression of BSD by identifying network architecture that distinguishes the BSD group from both the High-Risk and Low-Risk groups. Finally, it is possible that there are distinct patterns in the High-Risk group from both Low-Risk and BSD groups. This pattern of results would dissociate high reward sensitivity from moderate reward sensitivity, and healthy reward sensitivity from distinct mechanisms underlying BSD. While high-risk models address critical gaps in the literature, there is also room for methodological growth. In the next section, I describe the potential benefits of graph theory analyses to identify these correlates.

Graph Theory: Advantages of a Network Approach

Existing BSD literature largely describes the neurobiology of BSD in terms of structural or functional differences in sets of regions or pairwise comparisons of neural regions (Nusslock, Young, & Damme, 2014 for review). This approach presupposes a largely intact neural network with specific regional or pairwise disruption, without directly testing these network assumptions.

As a result, questions remain as to whether there is larger network dysfunction in BSD (Spielberg et al., 2016). Graph theory analyses provide a framework to directly test for large network structural abnormalities. Recent studies applying graph theory analyses show initial evidence that BSD is associated with abnormal neural network both functionally and structurally (Collin et al., 2016; Collin, Scholtens, Kahn, Hillegers, & van den Heuvel, 2017; Leow et al., 2013; Roberts et al., 2017; Spielberg et al., 2016; Wang et al., 2018). In the following section, I describe graph theory analyses in terms of levels of analyses, graph metrics, and network definition. Then, I discuss how graph theory analyses can be applied to diffusion-weighted structural data and resting-state functional data. Finally, I describe the few studies that have examined BSD with graph theory analyses.

Graph Theory Definition. Graph theory analysis is a mathematical framework to quantify properties of a network (Bullmore & Sporns, 2012; Zhang et al., 2011). A network is a system of interacting people or items. The items or people that comprise a system are referred to as nodes of that network, and the connections between nodes are referred to as edges. These edges are typically weighted or made binary based on the strength of the underlying relationships between nodes resulting in a network structure. Network structures are prevalent across many fields. As a result of this prevalence, graph theory analyses have been broadly applied to various network types including infrastructure (e.g., interstate and bridge systems), computational networks, and social networks. Regardless of the source of the network, graph theory analyses provide metrics that summarize features of the network, which provide insight into the whole system. These metrics typically focus on either the efficiency or structural features of the network. Efficiency describes the distance between nodes (e.g., path length) and relationships between nodes (e.g.,

clustering coefficients). Structural features focus on the similarity of the network structure either: across groups or to a model structure type (e.g., small world organization). Thus, graph theory analysis offers insights in the context of an entire network, beyond examining a limited set of brain regions or pairwise connections. Graph theory analyses also provide aggregate metrics that describe network features across three network definitions: whole brain network structures, subnetwork structures, and internetwork hub structure.

Graph Theory Levels of Analyses. Graph theory network topologies can be used to quantify many features of a network at several levels of analyses. Global graph theory metrics compare overall features of the network providing aggregate metrics of connections. These global metrics provide a broad insight into the whole network (e.g., network structure or network efficiency). Graph theory analyses also allow scientists to draw on established theoretical models to define subnetworks, or theoretically interrelated nodes of interest. By establishing subnetworks, graph theory quantifies the relationship between the nodes within theoretically defined subnetworks (Sporns, 2011). While global features of the entire network may be largely similar, specific nodal and subnetwork analyses can increase the specificity to detect more nuanced differences in critical networks. In this high-risk model, for example, it is possible that a reward sensitivity subnetwork would vary along a spectrum of risk for BSD, while the overall network structure of the brain is largely intact. In a single node region, graph theory quantifies the relationship of that node to critical subnetworks or the entire network. Frequently, single node regions are chosen because they play a critical integration role in a network, often referred to as a hub. These hub regions may play a critical role mediating the relationships between subnetworks, and any abnormality at this site could drive dysfunction for the network at large

(Bullmore & Sporns, 2009; Bullmore & Sporns, 2012). For example, some airports play critical hub roles in air travel networks as many flights connecting through that airport. Disruptions in proper function of critical hub airports, like a blizzard closing O'Hare, may cause widespread, downstream airline network disruptions. As previously discussed, past literature has largely examined single regions, or pairs of regions, assuming a largely intact network structure; I was able examine this assumption with network, subnetwork, pairwise, and regional correlates of BSD vulnerability or diagnosis with graph theory analyses. Graph theory analyses allowed me to examine whether the networks are in fact largely intact with limited regional abnormalities or if network abnormalities impact regional function. Taken together, graph theory analyses not only provide critical insight to a network, but it can also examine critical subnetwork and hub network features.

Critical Graph Theory Metrics. For the current project, the critical graph theory metrics include clustering coefficient, path length, and small world property. Clustering coefficient is calculated for each node and quantifies the number of connections between that node and its nearest neighbors over the maximum number of possible connections (Bullmore & Sporns, 2009, 2012; Sporns, 2011). At a network level, the average clustering coefficient provides an overview of the network structure. A random network, for example, would have low mean clustering coefficients, while complex biological systems typically display higher mean clustering coefficients (Bullmore & Sporns, 2009, 2012; Sporns, 2011). At a single hub or node level, this metric provides insight into how embedded a node is in its local network. In a social network, for example, an extroverted person would have a high clustering coefficient, communicating to all people around them. In contrast, an introverted person may have a low clustering coefficient,

interacting with a smaller set of their nearest neighbors. In the current study, emotion dysregulation in BSD could be caused by reduced clustering coefficient in emotion regulation regions as regulating regions are less embedded in an emotion neural network. Similarly, the reward hypersensitivity, that is associated with risk for BSD, may be related to reward-related brain regions having increased clustering coefficient (i.e., influence in their network). In summary, clustering coefficients provide insight into the connectivity of each node.

Another important metric is path length. Path length is the minimum number of edges (inter-node paths) that must be crossed to get from one node to another (Bullmore & Sporns, 2009, 2012; Sporns, 2011). This means that if each node in a network were directly connected to every other node, then the mean path length would be one path unit. An example of path length comes from a parlor game called the six degrees of Kevin Bacon. In this game players connect actors in a professional network to Kevin Bacon in six professional connections. Therefore, this game suggests that the node, Kevin Bacon, has a path length of six in a professional network. At the network level, average path length provides insight into a general structure and efficiency of the network. An efficient structure is considered a system with reduced path lengths. For example, if every town has an off-ramp on an interstate than the path length to the town would be fast and direct (a short path length). In contrast, if a town does not have a direct off-ramp then traffic would have to take back roads through other towns to get to their destination (a long path length). Random and complex networks have longer mean path lengths compared to linear and lattice network structures (Bullmore & Sporns, 2009). In terms of BSD, emotion dysregulation could result from increased path length in emotion regulation which would reduce the network ability to regulate emotion generation regions. Similarly, reward hypersensitivity may be related

to a reduced path length in the reward-related brain regions, which leads to an increased influence of reward on the larger neural network. While both clustering coefficient and path length metrics describe the relationship of a single node to other nodes in the network, they provide less insight into the overall structure of the network.

The overall structure of a network may be defined in terms of group differences spatially or in comparison to a model system structure (small world property). In line with cortical specialization, most graph theory studies reveal that cortical areas close together in space are functionally related and specialized. As a result, it is unsurprising that a growing literature reports a high small world property of the cortex (Bullmore & Sporns, 2009; Bullmore & Sporns, 2012; Sporns, 2011). A small world organization is defined by high levels of clustering among nodes of a network locally to form modular subnetworks with short paths that link all nodes of the network (Bullmore & Sporns, 2009). Small world property is a summary metric of the small world organization and is estimated in a two-step process. The first step is to simulate equivalent random networks to standardize the networks' clustering coefficients and the path lengths. Second, a ratio is calculated of the standardized clustering coefficient to the standardized path length (Bullmore & Sporns, 2009). In this way, small world property describes how closely a network adheres to a small world organization of specialized, local subnetworks that are typically connected through hub regions. These specialized subnetworks are not a unique proposal in the graph theory literature but are replicated across models of functional modularity in the brain (Zhang et al., 2011). The efficiency of a small world system emphasizes the importance of hub regions that integrate subnetworks into a small world organization, but small world property does not assess hubs directly.

Hub regions are nodes of high centrality between subnetworks, that increase the efficiency of the overall network by decreasing path length (Bullmore & Sporns, 2012). Both clustering coefficient and path length are used to measure the centrality of neural nodes. A central neural node has the shortest paths through it to all other network pairs in a network or subnetwork and a high clustering coefficient. These features make centrality a critical metric for hub regions that integrate information across networks (Bullmore & Sporns, 2009; Sporns, 2010). In summary, graph theoretical approaches provide measures of the relationship of a region to a network, the relationship between specialized subnetworks, and of the whole brain network. These network metrics, however, are heavily influenced by how the neural networks are defined.

Defining Networks Nodes. The accuracy of any model depends on the accuracy of the data upon which the model is formed. In graph theory, the accuracy of the network metrics is dependent on the accuracy of the network definition (Bullmore & Sporns, 2009; Fornito, Zalesky, & Breakspear, 2013). The network nodes must be meaningful units in the system (Fornito, Zalesky, & Breakspear, 2013). In some graph theory applications, the definition of a single node and an edge or path are apparent. In a social network, for example, the smallest meaningful node is a single person and the edge is a social interaction. In applications to neuroscience, the nodal assignment could take many forms. Although it could be argued that each node should represent a single neuron and each edge is a synapse, there is no reason to think that a cellular level of analyses is the most meaningful or relevant level of resolution (Fornito, Zalesky, & Breakspear, 2013). Examining the brain as a system brings a question as to the proper unit of definition of the nodes.

Recent applications of graph theory to BSD neuroimaging define nodes in one of three ways: resting state atlases/statistical independent atlas (GadElkarim et al., 2014; Roberts et al., 2017; Spielberg et al., 2016), standardized atlases (Forde et al., 2015; Manelis et al., 2016), or subject-specific segmentation (Collin, et al., 2016; GadElkarim et al., 2014; Leow et al., 2013). Resting state atlases or statistically independent atlases are frequently used to define nodes for resting state graph theory. An independent dataset is broken down into statistically independent or principle components masks, providing a statistical basis for the assumption that the nodes represent an independent, meaningful unit (O'Donoghue et al., 2017). This independent dataset can come from the current sample on a relevant task (Roberts et al., 2017), or based on outside, standardized resting state parcellation (GadElkarim et al., 2014; Spielberg, et al., 2016). While this statistical approach is widely accepted for resting state data, the relevance of functionally-defined statistical independence to structural analyses remains unclear.

Structural graph theory relies heavily on template-based or subject-specific anatomical definitions (O'Donoghue et al., 2017). Standardized templates are widely used, well studied, and highly reproducible. Despite these benefits, standardized templates have a critical limitation: a lack of anatomical specificity (Fornito & Bullmore, 2015). Although gross neuroanatomy is largely maintained across individuals, fine gyrification of the brain is unique to an individual (Zilles, Armstrong, Schleicher, & Kretschmann, 1988). Most standardized templates average across a large sample of individuals, which fits gross anatomy to an otherwise smooth brain obscuring anatomical specificity (Fornito & Bullmore, 2015). This lack of specificity is particularly critical in the question of node definition, as nodes must be optimally defined in graph theory analyses (O'Donoghue et al., 2017). Therefore, in structural graph theory analyses,

subject-specific parcellation maps present an attractive alternative. Subject-specific parcellation maps cortical parcellations onto the subjects' own anatomical images based on anatomical landmarks (Fischl, 2012). This approach has a high level of anatomic specificity and is widely preferred in structural graph theory analyses (O'Donoghue et al., 2017). Therefore, native space anatomical parcellation may be an optimal approach to define edges. In addition to defining nodes, a network is defined by edges which connect the nodes and define network architecture. Edge definition is closely tied to the type of connectivity measured (e.g., structural or functional). Thus, to define our edges, I must first consider our methodology.

Structural Graph Theory Analyses. Structural brain networks have largely been defined by anatomical tracings in empirical neuroscience (Bullmore & Sporns, 2009). Recent advancements in neuroimaging techniques allow neuroscientists to study the structural connectome in vivo with diffusion weighted imaging (Fornito, Zalesky, & Breakspear, 2013). Since brain tissue is highly organized, the directional flow of water molecules in a volumetric pixel (voxel) of that image can be informative about the content of that voxel (Seehaus et al., 2015). In white matter tissue, water molecules diffuse preferentially along axon bundles/myelin, and are limited by cellular structures in all tangential directions (Vollmar et al., 2010). Diffusion weighted imaging uses this directionality of water molecule diffusion to assess two features: orientation of white matter fibers (i.e., tensors) and metrics assessing the integrity of white matter within each voxel (e.g., fractional anisotropy).

During the processing of diffusion weighted imaging, the orientation of tensors is reconstructed based on a comparison of diffusion in all directions. If, for example, water molecules in a voxel diffuse strongly in an inferior to superior orientation and weakly in all other

orientations, then a tensor will be oriented in a superior-inferior orientation (i.e. the spinal cord). In addition to orientation, other diffusion metrics, such as fractional anisotropy, describe the distribution of this directional preference. Fractional anisotropy is a ratio that considers the primary anisotropic diffusion over the anisotropy in radial directions to provide a metric of the degree of diffusion direction. In highly directed white matter tissue, elevated fractional anisotropy values represent highly directed, anisotropic diffusion of water molecules. In large, highly myelinated tissue, such as the corpus callosum, the fractional anisotropy is high because molecules diffuse in a highly constrained right-left orientation. In contrast, water molecules diffuse freely in the ventricles leading to a low fractional anisotropy or isotropy. Fractional anisotropy provides insight into the microstructure integrity of the tissue underlying the voxel (Fornito, Zalesky, & Breakspear, 2013; Seehaus et al., 2015). In vitro, postmortem studies of DTI parameters related to direct measures of white matter, such as fiber density, axonal diameter, and myelination in specific white matter tracts (Seehaus et al., 2015). These metrics are not only informative of tissue structure, they can be used to define edges in structural networks (Fornito, Zalesky, & Breakspear, 2013; Leow et al., 2013; O'Donoghue et al., 2017).

In structural connectivity edges are typically defined in one of two ways: number of reconstructed tensors or fractional anisotropy (Fornito, Zalesky, & Breakspear, 2013; Leow et al., 2013; O'Donoghue et al., 2017). While no consensus exists on proper weighting, many studies suggest restricting edges based on the number of streamlines (Fornito, Zalesky, & Breakspear, 2013). However, the current BSD literature on structural graph theory analyses remains divided on whether to use fractional anisotropy (Collin et al., 2016; O'Donoghue et al., 2017) or number of tensors (Forde et al., 2015; GadElkarim et al., 2014; Leow et al., 2013) to

weight network edges. One problem with depending on the number of tensors is that the number of reconstructed tensors is an abstraction of the algorithm itself and depends less on the underlying tissue (Fornito, Zalesky, & Breakspear, 2013). In contrast, fractional anisotropy may be a preferable metric as research has validated that this metric reflects tissue features relevant to neurological disorders (Leow et al., 2013; O'Donoghue et al., 2017). To date, no similar anatomical validation exists for counts of tensors (O'Donoghue et al., 2017). Taken together, these points highlight that using fractional anisotropy would generate a more valid representation of the underlying anatomy.

Functional Graph Theory Analyses. Functional brain networks were defined for nearly a century by surface recordings of electrical neural activity with electroencephalogram. Recent advancements in neuroimaging techniques increase the spatial precision of the functional connectome by examining blood-oxygen level dependent (BOLD) signal in functional magnetic resonance imaging (fMRI). BOLD signal leverages the coupling between neuronal activity and hemodynamics (i.e., local control of blood flow and oxygenation) to provide an indirect metric of neural activity (Logothetis, 2003). BOLD signal relies on the distinct ferrous properties between oxyhemoglobin and deoxyhemoglobin in microvasculature innervating neural tissue. This relative concentration of hemoglobin is dependent on neural activity. Increased neural activity creates a metabolic demand for oxygen in the neural tissues and drives an increase in blood flow to replenish oxyhemoglobin. This increase in metabolic demand leads to a decrease in the concentration of deoxygenated hemoglobin in the microvasculature surrounding neural activity. This vascular change, in turn, leads to a change in BOLD signal (i.e. an increase in the level of non-paramagnetic oxygenated hemoglobin to paramagnetic deoxygenated hemoglobin;

Logothetis, 2003). Therefore, the BOLD signal is a reliable, but indirect measure of local neural activity that provides increased spatial resolution to in vivo measures of neural activity. Additionally, spontaneous resting-state fluctuations in BOLD activity provide a functional metric of neural connectivity.

In fMRI, spontaneous fluctuations in BOLD signal are measured during a resting-state, meaning the data is collected free from the constraints of a task (D'Esposito, Deouell, & Gazzaley, 2003; Fox & Raichle, 2007). In this way, resting-state fMRI (rs-fMRI) relies entirely on temporal correlation in spontaneous fluctuations of neural activity across the brain (Damoiseaux & Greicius, 2009; Fox & Raichle, 2007). These temporal correlations between regions reveal functional network patterns that relate to task evoked networks (Biswal, Zerrin Yetkin, Haughton, & Hyde, 1995; Shehzad et al., 2009) and structural connectivity (Andrews-Hanna, Reidler, Sepulcre, Poulin, & Buckner, 2010; Carver, Johnson, Joormann, Kim, & Nam, 2011; Damoiseaux & Greicius, 2009; Greicius, Supekar, Menon, & Dougherty, 2009; Leow et al., 2013; Poldrack et al., 2015). As a result, it is possible that structural connectivity relates to functional connectivity – that is, regions that are physically connected should be functionally connected. However, rs-fMRI may reveal connectivity beyond anatomically defined networks. Though spontaneous activity in underlying rs-fMRI connectivity relates closely to structural connectivity (Deco et al., 2013; Deco, Jirsa, & McIntosh, 2011; Poldrack et al., 2015), there are indirect connections that are also highlighted in rs-fMRI that may provide critical insight into network function. These discrepancies between resting state connectivity and underlying anatomy has led to some skepticism of the validity of rs-fMRI networks. However, these resting-state network analyses produce consistent results across subjects (Damoiseaux et al., 2006) and

in multiple measures of reliability (Braun et al., 2012; Shehzad et al., 2009). Specifically, rs-fMRI is reliable in terms of test-retest (Shehzad et al., 2009), interclass coefficient (Braun et al., 2012; Shehzad et al., 2009), and longitudinally in a single subject (Poldrack et al., 2015). This reliability is particularly strong when these rs-fMRI correlations are analyzed as edges or global metrics in graph theoretical approaches (Braun et al., 2012; Poldrack et al., 2015). From these converging measures, it can be concluded that this spontaneous activity reflects functional networks.

In network analyses of rs-fMRI, the edges are defined as the correlation between the nodes (Bassett & Sporns, 2017). While the definition of edges is widely accepted across the field, the proper level to threshold these edges remains contentious. Correlation coefficients, or functional edges, are thresholded to leave only the most robust, highest correlation coefficient (Sacchet et al., 2016; Sporns, 2011). Across the literature, the thresholding typically retains the top 20-30% of edge weights (Braun et al., 2012; Sacchet et al., 2016; Sporns, 2011). Although a lower percentage would be a more conservative estimate of functional network edges, thresholds below 25% are less reliable in repeated measure assessments (Braun et al., 2012). Thresholding coefficients above 25%, however, may generate results that are outside of biological plausibility (Sacchet et al., 2016; Sporns, 2011). Furthermore, reliability is reduced when using a threshold above 30% (Braun et al., 2012). Thus, though there is no clear consensus in the literature on the proper level of threshold in rs-fMRI, to address this issue many researchers examine the network structures in a range from 20% to 30% thresholding to examine a full range of biologically plausible networks (Collins et al., 2017), and interpret only regions that are stable across the biologically feasible threshold.

BSD Graph Theory Literature. While only a handful of studies have examined BSD using graph theory analyses, already the methodology is providing converging evidence of both structural and functional whole brain network abnormalities in BSD (Collin et al., 2016; Collin, Scholtens, Kahn, Hillegers, & van den Heuvel, 2017; Leow et al., 2013; Roberts et al., 2017; Spielberg et al., 2016; Wang et al., 2018). BSD is associated with decreased clustering coefficient in both structural (Leow et al., 2013) and functional (Roberts et al., 2017; Wang et al., 2018) network architecture. Reduced clustering coefficient means that the average neural node is less connected to neighboring regions in BSD compared to healthy controls. Thus, it is unsurprising that BSD is also associated with reduced global efficiency (Collin et al., 2016; Leow et al., 2013; Spielberg et al., 2016). Global efficiency is the average inverse shortest path length (Bullemore & Spoorns, 2009; Rubinov & Spoorns, 2010), meaning in BSD global path length is long, leading to the global efficiency being low. Reduced global efficiency or increased path length have been found in both structural (Collin et al., 2016; Leow et al., 2013) and resting-state functional network analyses (Spielberg et al., 2016) in BSD. Thus, graph metrics suggest that BSD is associated with a global reduction in the coordination of regions locally (clustering coefficient) and reduced efficiency between regions (path length). This is true for how regions physically connect (structurally) and how regions communicate (functionally). While informative of the overall structure, these global metrics lack the specificity of where and how these network differences occur, and therefore nodal graph metrics were also compared.

In nodal graph metric comparisons, the neural architecture at each node is compared in a thresholded network map to identify sites of abnormal network structure. Nodal comparisons of neural architecture in individuals with a BSD have found a distinct pattern of network

architecture both structurally (Leow et al., 2013) and functionally at rest (Spielberg et al., 2016). Structurally, individuals with bipolar disorder have an increased clustering coefficient in the left hippocampus, right cingulate, and right lOFC structurally (Leow et al., 2013). Functionally, individuals with a BSD have an increased clustering coefficient in the right amygdala (Spielberg et al., 2016), right superior middle frontal gyrus (Forde et al., 2015) and left middle frontal gyrus (Forde et al., 2015) at rest. Taken together, these findings suggest that frontal the cortex and critical subcortical regions (such as the hippocampus and amygdala) may play critical roles in the pathophysiology of BSD (Forde et al., 2015; Leow et al., 2013; Spielberg et al., 2016). The sensitivity of these findings, however, may be further increased if neural nodes are considered inside theoretically defined subnetworks rather than in an exploratory whole brain approach.

Current BSD literature has largely taken an exploratory approach to examining network structure, although there are three notable exceptions to this approach (GadElkarim et al., 2014; Manelis et al., 2016; Wang et al., 2018). GadElkarim et al. (2014) examined a default mode subnetwork, finding a distinct network structure in BSD, particularly in default mode regions such as the bilateral paracentral gyrus and right medial orbitofrontal cortex. While these findings provide critical insight into the function of a statistically, functionally distinct network, the relevance of that default mode network connectivity in the identification and course of BSD remains unclear. Similarly, Wang et al. (2017) found no global metric or whole brain differences in patients with bipolar disorder but did find limbic network and Default Mode Network differences associated with BSD. In a similar subnetwork approach, Manelis et al. (2016), defined distinctly defined bottom-up and top-down subnetworks to examine the structural architecture of reward anticipation during a task comparing individuals with bipolar disorder to

individuals with depression and healthy controls. Manelis et al. (2016) found that BSD was associated with denser subnetwork connectivity during reward anticipation and sparser subnetwork connectivity during loss anticipation. While this provides intriguing evidence of abnormal reward processing in BSD, it provides little insight into the stable, task-free structural and functional mechanisms driving these process differences and potentially this disorder. Indeed, foundational work is needed examining these BSD relevant subnetworks both in terms of structure and resting-state architecture.

In summary, graph theoretical approaches provide unique insight into network structure on several levels of analyses, moving beyond regional and pairwise network approaches to examine network features. This nodal to global network level flexibility makes graph theory analyses a critical analytic approach to test theoretical network models as it can examine both network level and regional hypotheses simultaneously. While only a handful of studies have examined BSD with graph theory analyses, these studies have largely taken an exploratory approach (Collin et al., 2016; Collin, Scholtens, Kahn, Hillegers, & van den Heuvel, 2017; GadElkarim et al., 2014; Leow et al., 2013; Spielberg et al., 2016; Wang et al., 2018). Taking an exploratory approach fails to build neurobiological models of BSD. Many of these exploratory models identified network differences in regions that are theoretically critical sites of emotion generation/regulation, and reward sensitivity subnetworks (Forde et al., 2015; GadElkarim et al., 2014; Leow et al., 2013; Roberts et al., 2017; Spielberg et al., 2016). However, no study has examined these models or neural regions directly in a graph theoretical approach. Thus, this project is the first to directly test the network models proposed in the reward hypersensitivity model and the emotion generation/regulation literature in participants with and at risk for a BSD.

The present study is the first to examine a behavioral high-risk model at a network level (although see Collin, Scholtens, Kahn, Hillegers, & van den Heuvel, 2017; Forde et al., 2015; Roberts et al., 2017 for genetic high-risk models). In the following sections, I summarize the neural network models proposed in both the reward hypersensitivity model and the emotion regulation literature, respectively. Then, I integrate these models to create theoretically defined subnetworks and critical hubs.

Theories of BSD Subnetworks and Integrative Hubs

In the current study, graph metrics were compared in three network definitions: a whole brain network, an emotion generation/regulation subnetwork, and a reward subnetwork. The theoretically defined subnetwork models (emotion generation/regulation and reward subnetworks) draw on neurobiological models of BSD. Two primary neural network models of BSD focus on reward sensitivity and emotional dysregulation (Mayberg, 1997; Merchand, 2011; Phillips, Ladouceur, & Drevets, 2008; Strakowski et al., 2012). In addition to the whole brain network definition, examining both the reward hypersensitivity and emotion generation/regulation neurobiological models may increase sensitivity to theoretically relevant network changes. In the following section, I provide an argument for examining both the emotion generation/regulation and reward models. Then, I define each neurobiological model of BSD (emotion generation/regulation network and reward). Finally, I identify theoretically critical hub regions where emotion regulation and generation signal converge.

There are several reasons that examining both the reward hypersensitivity and emotion generation/regulation neurobiological models may provide a more comprehensive perspective BSD risk, as each model provides a unique complimentary perspective of BSD risk. While the

reward hypersensitivity model has provided insight into BSD, it is primarily focused on the reward sensitivity in BSD and less on the potential contributions of both emotion generation and emotion regulation. In contrast, emotion regulation models focus on interactions between emotion generation and emotion regulation. While emotion regulation models have provided insight into emotion dysregulation in BSD, they have typically not focused on the reward sensitivity that is predictive of bipolar episodes, particularly hypo/mania. As each network model targets a single feature of BSD (i.e., sensitivity to reward stimuli or emotion regulation) these models may provide an incomplete picture of BSD. Therefore, examining the neural subnetworks proposed in both of these models provides a more comprehensive and integrative model of BSD.

Another difference between these network definitions is the size of the network. The emotion generation/regulation model describes a broader network compared to the reward hypersensitivity model. The reward sensitivity model focuses on a smaller number of nodes that are embedded within the larger emotion generation/regulation network. Given the predictive power of reward hypersensitivity, focusing on nodes that may be particularly relevant to reward may increase sensitivity to corollaries of BSD risk. Similarly, as only the BSD group is experiencing significant emotion dysregulation, the emotion generation/regulation may identify corollaries of BSD. Additionally, restricting network definition from a larger emotion generation/regulation network to a selective reward network may increase sensitivity to network differences between groups. This is comparable to past research which has shown that moving from a whole brain network to theoretically defined networks increased sensitivity in past work

(GadElkarim et al., 2014; Manelis et al., 2016; Wang et al., 2018). Combining these two approaches may increase model sensitivity to relevant BSD abnormalities.

These theoretical subnetwork and hub analyses in the current study contributes to the field in several ways. First, this study was the first time these network models were directly examined in a network approach rather than integrating across incomplete information provided by region of interest analyses and pairwise connectivity. Second, by restricting the network definition from a whole brain analyses to theoretically relevant subnetworks may increase sensitivity to BSD relevant group differences. Third, by examining both models, these analyses provide comprehensive insight, and may additionally increase sensitivity by moving from the larger model of emotion regulation to the smaller reward sensitivity model. Finally, both the emotion regulation model and reward models describe regions where emotion regulation and generation signals converge, this study examined these regions directly to examine potential internetwork disturbances related to BSD. The following section reviews the neural network model of reward hypersensitivity model (for review Alloy & Nusslock, 2018; Nusslock, Young, & Damme, 2014) and the network models of emotion regulation. Then, I define two underlying subnetworks (reward sensitivity and emotional generation/regulation subnetworks) and critical hub regions based on the reward hypersensitivity and emotion regulation models.

Emotional Regulation Neurobiological Model of BSD. Emotional regulation is a process by which individuals modulate their emotional response in terms of emotion type, timing, experience, and expression (Gross, 2002). This emotional regulation process can be divided into two subnetworks: emotion generation and emotion regulation. Emotion generation subnetwork regions include amygdala (Phillips, Ladouceur, & Drevets, 2008), striatum (Haber & Knutson,

2010; Merchand, 2011), insula (Strakoski et al., 2012) and the limbic system (Mayberg, 1997). Emotion regulation subnetwork regions involve the frontal cortex, hippocampi, and portions of the cingulate cortex. In addition to these neural nodes interacting with respective reward and emotion generation/regulation subnetworks, these subnetworks interact with each other.

The emotion regulation subnetwork has direct action on the emotion generation network, balancing the competing forces of emotional reactions and cognitive context (Phillips, Ladouceur, & Drevets, 2008; Marchand et al., 2011). The emotion generation subnetwork also acts on the emotion regulation subnetwork by sending information to emotion regulation regions to inform higher level cognition, actions, or predictions of outcomes and environmental cues (Phillips, Ladouceur, & Drevets, 2008; Marchand, 2011). Both emotion generation and emotion regulation subnetworks may play critical roles in BSD dysregulation.

Emotion regulation is frequently described as originating in dorsal cortical regions including the dorsolateral prefrontal cortex (dlPFC), ventrolateral prefrontal cortex (vlPFC), dACC, and dorsomedial prefrontal cortex (dmPFC), which regulates emotional generation via the OFC to the amygdala and ventral striatum (Phillips, Ladouceur, & Drevets, 2008; Strakowski et al., 2012). In this way, many signals of emotion regulation converge on the OFC, which integrates this signal providing feedback to the amygdala and striatum. In contrast, the emotional generation pathway involves the VS, amygdala, insula, globus pallidus, and mOFC, among other regions. Responses from these regions then typically activate the dorsal anterior cingulate cortex (dACC) (Phillips, Ladouceur, & Drevets, 2008). From the dACC, the emotion generation regions interact with dorsal emotion regulation regions, including the dACC and dlPFC (Phillips, Ladouceur, & Drevets, 2008). This interactive process between emotion generation/regulation

regions emphasizes the possibility that emotion dysregulation could emerge in several ways. For example, it is plausible that emotion dysregulation may arise from aberrant integration of regulation signals in the OFC or a failure of emotion generation regions, such as the striatum and amygdala, to respond to the OFC signal. Taken together, emotion regulation neural network models suggest three theoretically critical internetwork hub sites in the OFC, striatum, and amygdala.

Reward Hypersensitivity Neural Network Model of BSD. The reward hypersensitivity model proposes that bipolar disorder is characterized by abnormalities in reward-related brain function in a corticostriatal circuit (see Nusslock, Young, & Damme, 2014 for review). The reward hypersensitivity model of BSD focuses on reward hypersensitivity because of its predictive value for both hypo/mania; involving reward regions are situated in neural networks that also involve emotional regulation (Phillips, Ladouceur, & Drevets, 2008; Strakowski et al., 2012; Mayberg, 1997). Both functional and structural evidence relate BSD to aberrant corticostriatal neural circuitry, which is central to the reward system (Haber & Behrens, 2014; Haber & Knutson, 2010; Kringelbach & Berridge, 2009; Schultz, 2000). The corticostriatal circuit involves neural projections from midbrain nuclei (i.e., the ventral tegmental area (VTA)) to subcortical regions that are central to processing the rewarding properties of stimuli, i.e, the ventral striatum. This circuitry continues to cortical target regions (e.g., the orbitofrontal cortex, medial prefrontal cortex, anterior cingulate cortex). Thus, the reward neural subnetwork originates in the VTA and sends projections to several cortical areas (dACC, lOFC, and mOFC) via a ventral striatal hub. In the reward hypersensitivity model, reward sensitivity is thought to be generated in subcortical regions (VTA and VS), and regulated by cortical regions (dACC, lOFC,

and mOFC). While these regions have been examined in isolation or in pairwise coupling (Damme, Young, & Nusslock, 2017), this approach leaves many questions unanswered as to the source of dysregulation.

Dysregulation of reward processing may arise from multiple sources. One potential source is that "bottom-up" emotional reactivity overwhelms regulation networks. In other words, elevated reward reactivity generated in the VTA and VS overwhelms cortical regulatory networks. Alternatively, deficits in regulatory systems may result in emotion generation systems being unregulated. Finally, interactions between these subnetworks at a critical hub region (i.e. ventral striatum) may be disrupted and drive emotion dysregulation. Examining neural regions in isolation provides incomplete insight into these network hypotheses and highlights the importance of a broader network perspective in BSD research. Accordingly, the reward hypersensitivity model of BSD could benefit from integrating insights from a parallel emotion regulation network literature. While the reward hypersensitivity model of BSD focuses on neural reactivity to reward stimuli, these emotional responses are embedded in an emotion regulation network. The emotion regulation network describes a broader set of neural regions involved in emotion generation and emotion regulation that includes the reward subnetwork inside a larger network structure. In the following sections, I describe emotion regulation neurobiological subnetworks.

Theoretical Subnetwork Conclusions. In summary, there is significant overlap in neural regions included the emotion regulation model and the reward hypersensitivity model. The emotion regulation literature provides a broader, complimentary neural network model to the reward hypersensitivity model. The emotion generation nodes include both subcortical regions

(VS) to add critical other emotion generation cortices (dACC, amygdala, mOFC, and insula). The emotion regulation literature identifies a larger involvement of the frontal lobe (dlPFC, vlPFC, dmPFC), and the cingulate cortex in addition to the OFC. In this way, the emotional regulation model of BSD expands both emotion generation and emotion regulation subnetworks to generate a broader network model of BSD. One problem with this approach, however, is that it describes emotion dysregulation broadly, and could apply to any mood disorder. Therefore, it is possible that the reward hypersensitivity model increases specificity to critical BSD circuitry by reducing the neural circuitry to the most relevant regions. By examining three theoretical subnetworks, this study was able to directly compare the sensitivity of these models to BSD neural network architecture. In the previous section, I define two theoretical subnetworks: reward and emotion generation/regulation. By examining two subnetworks, these analyses account for the distinguishing features of BSD, and directly test these neural subnetwork models for the first time.

Integrated Theoretical Subnetworks and Critical Integration Hubs. Both the reward hypersensitivity model and emotion generation/regulation literature provide complimentary accounts of critical neural networks. Each model highlights critical features that are central to BSD. The reward hypersensitivity model highlights sensitivity to reward as a distinguishing feature of BSD and provides a unique account of emotional sensitivity to reward in BSD (Nusslock, Young, & Damme, 2014). The emotion generation/regulation model emphasizes emotional dysregulation, and the important balance between emotion generation and emotion regulation (Phillips, Ladouceur, & Drevets, 2008). Together these models provide a comprehensive account of critical neural networks underlying the pathophysiology of BSD. In

the following section, I define three theoretical subnetwork integration hubs (VS, Amygdala, and OFC) for these analyses, while making a critical improvement on OFC node definition (medial OFC and lateral OFC). Namely, despite many researchers treating the OFC as a homogenous structure, I argue that the distinct roles of the lateral and medial OFC are critical to a comprehensive network understanding. Finally, I review evidence that these subnetworks and critical hub regions are aberrant in BSD structure and function across levels of severity and mood states.

Each of the network definitions (whole brain, emotion/generation, and reward) will be examined at the nodal level, but there may be added value by examining theoretically relevant internetwork hub regions in addition to nodal graph metrics. While nodal graph metrics analyses highlight critical nodes that differ within a specified network, these analyses assume that all nodes within a given network are largely of equal importance to that network. However, all nodes may not be equally important to the function of the network. There are, in fact, regions within networks where emotion regulation and emotion generation signal converge (i.e., theoretical internetwork hubs). While group differences within theoretical internetwork hubs may not differ compared to other regions within a network, they may still contribute to key emotion dysregulation. Given the role of theoretical internetwork hubs within the network, the implication of these group differences at these sites may be clinically and theoretically relevant. To illustrate this point, I refer to an analogous network: airline travel. While delays in arrival may not significantly differ between O'Hare Airport in Chicago, Illinois and Eppley Airfield in Omaha, Nebraska, the implications of delays are very different between these nodes. Delays at O'Hare Airport are more likely to impact other flights because O'Hare Airport is a critical site of

flight convergence, whereas delayed arrivals into Eppley Airfield may have less of impact on air travel in general. In this way, delays at each node in an air travel network should not be treated as equal. Similarly, there are regions that are critical sites of convergence for both emotion regulation and emotion generation. Although group difference at these sites may not be reflected in nodal metrics differences, they may critically contribute to emotion dysregulation. Accordingly, we examined critical theoretical internetwork hubs that may not appear in the nodal comparisons.

As previously defined in the subnetwork models, there are several critical nodes in which the reward and emotion generation subnetworks and emotion regulation subnetworks converge (including the OFC, Amygdala, and VS). These sites of convergence may represent critical sites of network dysregulation; reduced regulation or increased emotion generation at any of these sites may have downstream impacts on the entire network. For example, reduced connectivity between emotion regulation regions and the OFC may result in a failure of regulation of emotion generation regions, such as the VS and amygdala. Similarly, reduced connectivity from the OFC to the emotion generation regions (VS and amygdala) with increased connectivity to dACC may lead to increased "bottom-up" emotional generation without the appropriate emotional regulation. To account for these possibilities, I examine the path length and clustering coefficient at these critical nodes across the high-risk design with the modification that I divide the OFC into medial and lateral portions.

The OFC is frequently identified as a critical site of interaction between reward/emotion generation and regulation. However, the OFC is not a homogenous structure, but can be divided into medial and lateral portions with distinct functional roles and neural connectivity (Elliott,

Dolan, & Frith, 2000; Howard & Kahnt, 2017). The medial OFC (mOFC) is clearly sensitive to the rewarding properties of stimuli and the generation of positive or approach-related affect. In contrast, the lateral OFC (lOFC) is sensitive to both positive and negative (i.e., punishment) cues (Elliott, Dolan, & Frith, 2000). This broader sensitivity to both positive and negative cues suggests that the lOFC maintains a current reward value, both forming and updating changing reward values for a given stimulus (Elliott, Dolan, & Frith, 2000; Howard & Kahnt, 2017). Accordingly, activation of the lOFC has been interpreted in terms of arousal and salience (Elliott, Dolan, & Frith, 2000; Howard & Kahnt, 2017), as opposed to positive hedonic evaluation. Activation of the mOFC is related more directly to hedonic response, motivation, and reward pursuit. These OFC subregions also have distinct neural network connectivity. The mOFC receives primary and secondary sensory input, including direct connections from olfactory cortex, visual association cortex, and somatosensory cortex (Elliott, Dolan, & Frith, 2000; Kringelbach, 2005). The mOFC also receives modulating input from the lOFC and sends modulating output to the VS and the amygdala (Elliott, Dolan, & Frith, 2000; Kringelbach, 2005). The lOFC receives input from dorsal and anterior frontal regions and sends input to the mOFC. Taken together, the lOFC integrates critical emotion/reward regulation, while the mOFC sends direct input to the amygdala and ventral striatum to modulate emotion generation. Abnormalities in either the lOFC or mOFC may reflect disrupted emotion regulation processes responsible for mood instability (Phillips, Ladouceur, & Drevets, 2008). While disruptions in the mOFC would impact critical interface between emotion generation and emotion regulation, disruptions in lOFC would lead to a failure to integrate regulatory signal. Given these independent roles and connectivity it is critical to define the lOFC and mOFC as separate nodes

in these subnetworks and graph theory analyses. Therefore, this neural network model split the OFC into the mOFC and lOFC.

In summary, neurobiological models of BSD have defined critical regions where theoretical subnetworks converge. Due to this critical integrative role, these sites of subnetwork convergence may be critical to network dysregulation. Just as poor weather at O'Hare airport may cause airline delays nationwide, abnormal network efficiency in the lOFC, mOFC, VS, or amygdala may result in reduced emotional regulation or increased emotion generation. To account for this possibility, I examined the clustering coefficient and path length in these theoretical hub regions.

BSD Subnetwork and Integrative Hub Conclusions. Emotion dysregulation may arise from aberrant integration of regulation signals in the OFC or a failure of emotion generation regions, such as the striatum and amygdala, to respond to the OFC signal. Two subnetworks were investigated in these analyses: reward, emotional generation/regulation. The reward subnetwork included the VTA, VS, mOFC, lOFC, and dACC. Within the emotion generation/regulation subnetwork, the emotional generation subnetwork contained the VTA, VS, amygdala, insula, dACC, globus pallidus, and mOFC, and the emotional regulation subnetwork included the lOFC, dACC, dlPFC, vlPFC, and dmPFC. I also explored the critical internetwork integration hubs across these models including VS, lOFC, mOFC, and amygdala. Examining three neural subnetworks (whole brain, emotion generation/regulation, and reward) provides a more comprehensive model of BSD that may also increase sensitivity to BSD relevant network changes. These analyses have the added benefit of examining theoretical subnetwork models in a graph theoretical approach.

Current Study Design

This study used a behavioral high-risk design to examine structural and functional network architecture associated with BSD. This high-risk design included moderate reward sensitivity individuals at low-risk for BSD (Low-Risk), high reward sensitivity individuals who are at elevated risk for BSD but who do not have a lifetime BSD diagnoses (High-Risk), and high reward sensitivity individuals who have a BSD diagnosis (BSD). This 3-group design dissociate correlates of risk for BSD from correlates of the presence of BSD. Correlates of vulnerability appear in both the High-Risk and the BSD groups. Correlates of the presence or progression of BSD distinguished between BSD and High-Risk groups. Furthermore, these graph theoretical analyses examined network architecture implicated in risk for BSD across three network definitions: a) whole brain network composition, b) theoretically defined emotion generation/regulation subnetwork, and c) theoretically defined reward subnetwork. Within each of these network definitions, graph metrics were calculated as global metrics, nodal metrics, and theoretically defined internetwork hub regions (lOFC, mOFC, VS, and amygdala). Additionally, these two neurobiological models of BSD (i.e., the reward hypersensitivity and emotion regulation models) have yet to be directly examined in a network model. Rather, they have relied on partial information afforded to them by region of interest, traditional whole brain, and/or pairwise connectivity approaches. By using a graph theoretical approach, this project was able to directly examine the efficiency of the network architecture in these theoretical models.

I hypothesize that BSD would be associated with global differences in functional and structural neural network architecture in line with Leow et al. (2013). I also expect that in the emotion generation/regulation subnetworks, BSD would be associated with reduced efficiency

(increased path length and decreased clustering coefficient) in emotion regulation regions and increased efficiency (decreased path length and increased clustering coefficient) in emotion generation regions (Phillips, Ladouceur, & Drevets, 2008). Similarly, I expected that there would be greater efficiency (reduced path length and increased clustering coefficient) in reward related regions associated with risk for BSD because risk for BSD is associated with reward hypersensitivity (Alloy et al., 2012a; Alloy et al., 2012b). Furthermore, I excepted that the BSD group would have pronounced differences at theoretical internetwork hubs where emotion generation and emotion regulation networks converge. Finally, I expect structural and functional network architecture to largely converge. Therefore, I propose a set of hypotheses across structural and functional analyses.

Structural (Aim 1) and Functional (Aim 2) Network Architecture Hypotheses

In the following section, I provide a general overview of the parallel analyses that will be conducted in both structural and functional graph theory analyses. I describe analyses that will be conducted for each neural network definition (whole brain, emotion generation/regulation, and reward) and for each level of analyses (global metrics, nodal metrics, and internetwork hub levels). Next, I describe potential findings, and their interpretation. Finally, I describe my hypotheses. For ease of readership, hypotheses will be reiterated within the results section.

Whole Brain Network Structure. Overall global metrics of the neural network structure (i.e., clustering coefficient, path length, and small world property) were examined using diffusion tensor imaging and resting-state functional imaging across bipolar risk groups. If the High-Risk and BSD groups have similar network metrics that are distinct from the Low-Risk group, then this may reflect a correlate of risk for BSD. Likewise, network metrics in which the

BSD group is distinguished from the other two groups may represent a correlate of the presence of a BSD. Based on prior graph theoretical approaches in the BSD literature (Roberts et al., 2017), I predicted that the BSD group would have a decreased clustering coefficient, increased path length, and decreased small world property at the whole brain level. If these network features represent correlates of BSD I predict a similar pattern for the High-Risk Group. Conversely, if these features are a correlate BSD presence, I would not expect to see a similar pattern in the High-Risk group. Based on the current literature, it is unclear whether global metrics would be sensitive to BSD risk. Thus, the high-risk design allowed me to test these competing hypotheses.

Subnetwork Structure. The network metrics were assessed in two theoretically critical subnetworks: reward and emotional generation/regulation subnetworks. Graph theoretical approaches to BSD have yet to examine network metrics in these three subnetworks. As a result, support for these subnetworks has been largely defined by whole brain or pairwise connectivity. This study represents the first test of these neurobiological models of BSD on a network level. I expected that BSD would be associated with higher subnetwork cohesion in the in reward and emotion generation regions, defined by low path length and high clustering coefficients. I expected that BSD would be associated with lower efficiency in the emotion regulation regions, defined by high path length and low clustering coefficients. Critically, if these patterns for BSD in the emotional generation and emotional regulation subnetworks represent correlates of risk for BSD I would predicted a similar pattern in the High-Risk group. Conversely, if these features are a correlate of BSD presence, I would not expect to see a similar pattern in the High-Risk group. Given that a wealth of neuroimaging and electrophysiological data support that aberrant

subnetwork function precedes BSD onset as a correlate of risk for BSD (see Nusslock, Young, & Damme, 2014 for review), I expected that High-Risk and BSD groups would display similar network structure in reward sensitivity regions. Accordingly, I hypothesize that the High-Risk group would display increased clustering coefficient and decreased path length in emotion generation. In contrast, I expected decreased clustering coefficient and increased path length in emotion regulation subnetworks, compared to the Low-Risk group.

Internetwork Hub Regions. The network metrics discussed above would also be assessed in four theoretically critical hubs: lOFC, mOFC, VS, and amygdala. Graph theoretical approaches to BSD have yet to examine network metrics in these three subnetwork hubs. I expected that BSD would be associated with higher clustering coefficient and lower path length in emotion generation hubs (i.e., mOFC, VS and amygdala). I hypothesized that deficits in internetwork integration would be related to the integration of regulation in the lOFC or to the direct modulatory input from the mOFC to VS and amygdala would be observed in both the BSD and High-Risk groups.

Methods

Longitudinal Study Participants and Recruitment Procedures. The analyses were conducted on already collected data from an NIH funded longitudinal investigation of reward-related brain function and risk for BSD directed by Lauren Alloy and Robin Nusslock. Participants were recruited via a two-stage screening procedure (Alloy et al., 2012b). In the first step, 9,991 students (ages 14-19) from the Philadelphia area completed two measures: Carver and White's Behavioral Inhibition System/Behavioral Activation System scales (BIS/BAS; Carver & White, 1994) and the Sensitivity to Punishment/Sensitivity to Reward Questionnaire

(SPSRQ; Torrubia, Ávila, Moltó, & Caseras, 2001). These measures were used to define cut-offs for moderate reward sensitivity (Low-Risk) and high reward sensitivity (High-Risk). Participants between the 40th to 60th percentile on both the Total BAS subscale of the BIS/BAS scales and the Reward subscale of the SPSRQ were classified as moderate reward sensitivity and considered low risk for BSD (n = 750). Participants scoring in the 85th to 100th percentile on both measures were classified as high reward, high risk for BSD (n = 1,200). From this initial screening, 539 individuals (334 high reward and 205 moderate reward) returned for the Phase II screening.

Phase II screening involved a semi-structured diagnostic interview using the expanded Schedule for Affective Disorders and Schizophrenia- Lifetime interview (exp-SADS-L; Alloy et al., 2012b; Endicott & Spitzer, 1978). The exp-SADS-L was used to classify individuals as having a BSD and gathered information about clinical features including: number of depression episodes, number of mania episodes, age of first manic episodes, and age of first depressed episode. Additionally, the exp-SADS-L assessed for the presence of other disorders. Participants were excluded from the final sample if they had a primary psychotic disorder (n = 7) or were not fluent in English (n = 5). Finally, to begin the longitudinal phase participants, were invited to complete a baseline assessment, which included questionnaires, behavioral tasks, and additional diagnostic and life stress interviews. At baseline, the study included 486 participants (300 high reward and 176 moderate reward). Participants enrolled in this study then completed regular prospective assessments at approximately 6-month intervals over a period of up to five years.

Neuroimaging Study Participants. A subset of participants (ages 18 and over) were invited to participate in the MRI study if they did not meet further MRI exclusion criteria

involving the presence of ferrous metal in any part of the body, head trauma, claustrophobia, left-handedness, or pregnancy. Participants provided informed written consent and were compensated $100. All protocols were approved by the IRB at Temple University. A total of 131 participants (52% female) ranging in age from 18-27 completed the MRI portion of the study (Table 1). This sample included 44 Low-Risk individuals, 53 High-Risk individuals, and 34 individuals with a bipolar spectrum diagnosis (BSD). Within the 34 individuals in the BSD group there were a range of diagnoses, including 3 individuals with cyclothymia, 18 individuals with a bipolar II disorder, 4 with bipolar I disorder, and 9 with bipolar disorder not otherwise specified. In line with recruitment goals of the high-risk design, the Low-Risk participants had significantly lower reward sensitivity than both the High-Risk group and the BSD group on both the Sensitivity to Reward Subscale and BAS Total (Table 2).

Although I excluded for the presence of psychotic disorders, all groups could have lifetime diagnoses of unipolar depression, anxiety disorders, post-traumatic stress disorder, attention deficit hyperactivity disorder, substance use disorder, eating disorder, and/or obsessive-compulsive disorder. In fact, every group had some lifetime non-BSD clinical diagnoses: 26 Low-Risk individuals, 40 High-Risk individuals, and 20 BSD individuals. Across groups, there was no significant difference in the presence of non-BSD diagnoses; except unipolar depression and ADHD. Along with the presence of psychiatric diagnoses, there was medication use across all three groups as well. There was no significant difference across groups in the number of individuals taking psychiatric medications (SSRIs, Tricyclics, Lithium, etc.) (Table 3). In terms of current diagnoses, there were 11 current major depression episodes across all three groups: 1 Low-Risk individual, 6 High-Risk individuals, and 4 BSD individuals. In the BSD group, current

mood states at time of the scan varied with 26 individuals in a euthymic or remitted state, 4 individuals in a depression episode, 4 in a current hypomanic episode, and no participants were in a current manic mood episode.

MRI Data Acquisition. All MRI data were collected on a 3T Verio MR scanner (Siemens, Erlangen, Germany) at Temple University. Structural images were collected in a T1-weighted anatomical image (sagittal plane; repetition time [TR] 1,600 ms; echo time [TE]2.46 ms; .5 mm3 isomorphic voxels, 176 interleaved slices; FOV 515; flip angle 57). Diffusion weighted images were collected in axial brain slices were collected with the following parameters: 64 diffusion-weighted (b = 1000 sec/mm2) and 1 non-diffusion weighted scan; field of view 190×190 mm; voxel size 2×2×2 mm; repetition time = 9900 msec; echo time = 90 msec. For the resting state scan, gradient echo-planar imaging (EPI) was used to acquire a series of 300 T2*-weighted functional images with the following parameters: 35 oblique transverse slices collected in interleaved descending order, repetition time (TR) = 2.00 s, echo time (TE) = 20 ms, flip angle 70°, FOV 384 x 384 mm, matrix 104 x 104, 4 mm slice thickness with no gap, voxel size = 3.7 x 3.7 x 4.0 mm. A rear-projection system was used for all stimulus presentation, and behavioral responses were collected using a response pad.

Structural Preprocessing. FreeSurfer version 5.3.0 automatic segmentation software extracted surfaces (http://surfer.nmr.mgh.harvard.edu/; Fischl et al., 2002). Specifically, morphometric measurements were obtained by reconstructing representations of the gray/white matter boundaries. Using cortical folding patterns native space anatomical labels were generated to maximize the accuracy of the morphological alignment of homologous cortical locations based on individually defined anatomical landmarks, while minimizing metric distortion. The

software segmentation moves the Desikan-Killiany Atlas into the subject's native space using anatomical landmarks.

Diffusion Preprocessing. Diffusion preprocessing corrected for field heterogeneities detected in the initial unweighted image, eddy current, masked the brain, and extracted the skull using the FMRIB Software Library's (FSL). Fractional anisotropy (FA) was computed on a voxel-wise basis using a single-tensor diffusion model. An optimized global probabilistic tractography method estimated whole-brain tractography. A total of 45,000 fibers were estimated for each participant. The FreeSurfer segmentation were registered (bbregister) to create a transformation matrix by registering the high resolution with the extracted unweighted brain image. This transformation matrix was applied to the cortical and subcortical automatic segmentation labels, which moved the labels from MPRAGE to the diffusion matrix dimensions and created the seed regions for the tractography in diffusion native space using TRActs Constrained by UnderLying Anatomy (TRACULA) toolbox. The labels were visually inspected for each subject, resulting in 68 unique cortical regions per participant. Nodes were placed in the center of each label. Structural connections were constructed in DTIStudio; fiber tracts were reconstructed by seeding at every voxel inside the brain. Fibers were assigned by continuous tracking algorithm until either the fiber bending angle exceeds 60^{o} of the FA drops below .25 (http://www.mristudio.org). These construction procedures are in line with many of the preprocessing procedures in recent graph theory applications (Collin et al., 2016; Leow et al., 2013; GadElkarim et al., 2014; Sacchet et al., 2016).

Resting Preprocessing. Functional data were preprocessed using FMRI Software Library 5.0.4 (http://www.fmrib.ox.ac.uk/fsl). I discarded the first 4 images to allow

magnetization equilibrium. The FreeSurfer segmentation used boundary-based registration (bbregister) by creating a transformation matrix and registering the high resolution with the extracted unweighted brain image. This transformation matrix was applied to the cortical and subcortical automatic segmentation labels, which moved the labels from MPRAGE to the diffusion matrix dimensions and created the seed regions for the tractography in resting state native space using the FreeSurfer Functional Analyses Stream (FSFAST) toolbox. The labels were visually inspected for each subject, resulting in 68 unique cortical regions per participant. Nodes were placed in the center of each label. Using segmentation from FreeSurfer, masks were used to remove white matter, cerebrospinal fluid, and temporal derivatives with linear regression. The FreeSurfer pial/white-matter surfaces were eroded prior to extracting time-series for de-noising. Motion scrubbing were removed time points with either framewise displacement (FD) 3 mm. Data were motion-corrected using the Motion-corrected Linear Image Registration Tool (McFLIRT), prior to band-pass filtering (0.008–0.08 Hz). Nodes were set in the center of each FreeSurfer label for each subject's rsfMRI time-series data, all pairwise Pearson correlation coefficients between nodes were calculated.

Graph Theory Edge Definition. For each participant, in native space, connectivity matrices were created using the 68 nodes (34 by hemisphere) FreeSurfer Desikan–Killiany atlas. This resulted in a 68 x 68 connectivity matrix for each participant, with each row and column representing a cortical region, and each cell element representing an edge between the corresponding cortical regions. The edge weights were calculated by distinct features in each modality (i.e., resting state functional images and diffusion weighted images). In the structural analyses, fractional anisotropy underlying each pair of regions were used as edge weights (Collin

et al., 2016; Sacchet at al., 2016). In functional analyses, edges are defined by pairwise Pearson's correlations across nodes relating the time course of spontaneous activity (Spielberg et al., 2016). These edges were defined using the umpc toolbox (Brown, 2018). From these matrices, graphs were derived for each subject. To make the matrices comparable across subjects, I applied a threshold such that only the 20-30% most robust edge weights were retained (Sacchet at al., 2016; Sporns, 2011). In line with recent approaches (Collins et al., 2017) I only interpret those findings that are consistent across a majority of that range (greater than 5% of the 20-30% range). As the reliability of central graph theory metrics (e.g., path length, clustering coefficient, etc.) is reduced at thresholds lower than 25% (Dennis et al., 2012). For small world property analyses, the matrices were binarized such that non-zero remaining edge weights were set to 1. This resulted in undirected graph for each subject. These binarized graphs were analyzed in the Brain Connectivity Toolbox (Rubinov & Sporns, 2010) with the GraphVar graphic user interface (Kruschwitz, List, Waller, Rubinov & Walter, 2015). This toolbox directly compared the network organization structurally and functionally. Additionally, the Brain Connectivity Toolbox was used to generate the critical graph theory metrics: clustering coefficient, path length, and small world property (see Rubinov & Sporns, 2010 for review). All raw graph figures were generated using the BrainModulyzer Software (Murugesan et al., 2017).

Accounting for Clinical Features of the Disorder. Follow-up analyses were conducted only in significant network effects of the neural network features to reduce the total number of comparisons. If findings appeared to be correlates of BSD, they were compared to self-reported symptoms across all groups, and features of BSD progression in the BSD group only. If findings appeared to be a corollary of risk, then they were compared to continuous measures of risk (BAS

and SR). In the BSD group, potential correlates of BSD presence or progression, were related to the lifetime number of mania episodes, the lifetime number of depression episodes, age of first depression episode, and age of first depression episode taken from the SADS-L (described above in the longitudinal screening section).

Variables of Potential Confounding Impact. Although potentially confounding features were largely excluded from this study by design, there remain some variables that must be explored for their potential confounding impact. These variables include age, sex, and psychiatric medication status. While there is no indication of a group differences among these variables, each of these variables may be related to the neural network structure. Early adulthood, for example, is a time of frontal lobe maturation; although age may not statistically differ among groups, the impact of age on frontal lobe network structure may vary across groups (Lebel et al., 2008). Therefore, the impact of these variables on large-scale brain networks were compared to the primary global metrics (clustering coefficient, path length, and small world property) in a linear model, and included as covariates if significantly related to network metrics.

Data Analytics: Structural (Aim 1) and Functional (Aim 2) Network Architecture

In the following section, I provide a general overview of the parallel graph theory analyses that were conducted in both structural and functional networks across three network definitions (whole brain, emotion generation/regulation, and reward). Analyses are described by level of analysis: global metrics, nodal metrics, and internetwork hub levels. First, I describe the models for each level of analysis. Next, I describe how correction for multiple comparisons will be calculated for each level of analysis. Finally, I describe follow-up analyses. For ease of readership, analytic strategies are reiterated within the results section.

Global Graph Metrics. First, separate analyses examined if global metrics vary by potentially confounding variables (sex, age, and psychiatric medication status). To reduce the total number of model parameters, potential confounding variables were only added to the model if they varied with the graph metric of interest. Global metrics of the neural network structure (clustering coefficient, path length, and small world property) were extracted from both resting state and diffusion data. These three metrics were compared across the three groups (Low-Risk, High-Risk, and BSD) in an ANCOVA, correcting for relevant confounding variables (sex, age, and psychiatric medication status). Within global graph metric analyses, the omnibus will only be considered significant if it survives Bonferroni correction for each for three comparisons (clustering coefficient, path length, and small world property) in the whole brain network ($p<.017$) and two comparisons (clustering coefficient and path length) in theoretical subnetworks ($p<.025$). Significant main effects or interactive effects of group were then examined in pairwise comparisons between each group. Pairwise corrections were corrected using the logic of Fisher's protected t-tests to minimize familywise error rate, which requires a significant omnibus test in order to proceed to or interpret follow-up tests. To reduce the total number of follow-up comparisons, follow-up analyses were conducted for any significant group differences based on the pattern of results (corollary of risk or corollary of BSD). For findings that were consistent with a corollary of risk, the global metrics were compared to continuous risk measures (BAS and SR) within the High-Risk and BSD group and were Bonferroni corrected for two comparisons ($p<.025$). For findings that were consistent with a corollary of BSD, global metrics were compared to clinical features (age of onset and number of episodes) within the BSD group were Bonferroni corrected for two comparisons ($p<.025$).

Nodal Graph Metrics. Nodal network organization was compared across the three groups (Low-Risk, High-Risk, and BSD) to identify areas of significant structural differences. In global and hub analyses graph metrics were extracted and compared across groups, but in nodal graph metrics, network-based statistics were conducted within the GraphVar suite to identify nodes where network structure differed by group (Kruschwitz, List, Waller, Rubinov, & Walter, 2015). These analyses are comparable to functional contrast analyses, in that a null finding results in no identified nodes or relevant statistics. As a result, any null findings were simply reported as finding no significant nodes with no corresponding statistics to report. The whole brain analysis was not restricted by a theoretical framework, as in the subnetwork analyses, and as such this nodal analysis was exploratory using a False Discovery Rate correction. The subnetwork analyses were restricted on a theoretical basis and corrected for using a random network permutation-based method to control familywise error (FWE). To reduce the total number of follow-up comparisons, follow-up analyses were conducted for any significant group differences based on the pattern of results (corollary of risk or corollary of BSD). For findings that were consistent with a corollary of risk, the nodal metrics were compared to continuous risk measures (BAS and SR) were Bonferroni corrected for two comparisons ($p<.025$). For findings that were consistent with a corollary of BSD, nodal metrics were compared to clinical features (age of onset and number of episodes) were Bonferroni corrected for two comparisons ($p<.025$).

Internetwork Hub Graph Metrics. For each theoretically identified hub (lOFC, mOFC, VS, and amygdala) I extracted two metrics: clustering coefficient and path length from the theoretically defined networks. Separate analyses examined if hub graph metrics vary by potentially confounding variables (sex, age, and psychiatric medication status). To reduce model

parameters, potential confounding variables were only added to the model if they varied with the graph metric of interest. Internetwork hub metrics were compared across the three groups: Low-Risk, High-Risk, and BSD in an ANCOVA, correcting for appropriate confounding variables. Internetwork hubs analyses were corrected for the four regional comparisons per network definition using Bonferroni correction (p=.0125) and treated separately for diffusion tensor analyses and resting state analyses. To reduce the total number of follow-up comparisons, follow-up analyses were conducted for any significant group differences based on the pattern of results (corollary of risk or corollary of BSD). For findings that were consistent with a corollary of risk, the hub metrics were compared to continuous risk measures (BAS and SR) within the High-Risk and BSD group and were Bonferroni corrected for two comparisons (p<.025). For findings that were consistent with a corollary of BSD, hub metrics were compared to clinical features (age of onset and number of episodes) with in the BSD group and were Bonferroni corrected for two comparisons (p<.025).

Structural Graph Theory Results

This section examines structural network architecture in BSD behavioral high-risk design across three network definitions (whole brain, emotion generation/regulation, and reward) using both global and nodal metrics. The high-risk design dissociated correlates of risk for BSD from correlates of BSD onset or progression. Correlates of risk for BSD were defined as significant differences that appear in both the High-Risk and the BSD groups. A correlate of risk may appear as an intermediate endophenotype between BSD and Low-Risk groups or where the High-Risk group does not differ from the BSD group. Correlates of the presence or progression of BSD were defined as significant differences that distinguish between the BSD and the High-

Risk groups. Furthermore, these graph theoretical analyses examined network architecture implicated in risk for BSD across three network definitions: (a) whole brain, (b) emotion generation/regulation subnetwork, and (c) reward subnetwork. These networks were examined in terms of global graph metrics, nodal graph metrics, and theoretical inter-network hubs. Finally, these two models of BSD (i.e., the reward hypersensitivity and emotion generation/regulation models) have yet to be directly examined as network structures; the following analyses are the first to examine these theories directly in terms of structural networks.

Structural Participant Demographics. I excluded nine individuals from structural (DTI) graph analyses based on motion artifact as assessed by visual inspection of reconstructed data. The final analytic sample for structural graph analyses was 121 (52% female) participants. This sample included 39 Low-Risk individuals, 51 High-Risk individuals, and 31 individuals with a bipolar spectrum diagnosis (BSD). The average age was 21 (SD = 1.94), and there was no significant group difference in age, $F(2,120) = 1.47$, $p = .24$. There was no significant difference in the ratio of sex across groups, $\chi^2(2) = 0.34$, $p = .84$. In all groups there were individuals taking psychiatric medications (e.g., antidepressants, benzodiazepines): 6 in the Low-Risk group, 6 in the High-Risk group, and 4 in the BSD group. There were no significant differences in the incidence of psychiatric medication status between these groups, $\chi^2(2) = 0.26$, $p = .88$.

Whole Brain Structural Network Analyses. In the following analyses subsection, global metrics of structural connectivity were extracted from the whole brain connectivity matrices where edges were defined by mean fractional anisotropy between nodes. The potential confounding effects of age, sex and psychiatric medication status were evaluated in separate analyses that examined their relationship to global graph metrics for these effects. Confounding

variables were included in group analyses if they related to the graph metric. Global graph metrics were then evaluated in three separate analyses of variances (ANOVAs) comparing group (Low-Risk, High-Risk, and BSD) in each graph metric (clustering coefficient, path length, and small world property). Nodal graph metrics (clustering coefficient and path length) were also calculated for each node to evaluate whether there were differences in these graph metrics for any node within the network. At the whole brain level nodal analyses were unrestricted by theory (i.e., exploratory) as such these analyses were corrected using False Discovery Rate (FDR). Nodal metrics were also assessed across the high-risk design in critical internetwork hub regions (lOFC, mOFC, VS (FreeSurfer label defined as nucleus accumbens), amygdala) using repeated measure general linear models.

Whole Brain Graph Theory Global Metrics. Separate analyses evaluated potential relationships to the global graph metrics (clustering coefficient, path length, and small world property) to age, sex, and psychiatric medication status. Clustering coefficient and path length global graph metrics were not related to age, sex, and psychiatric medication status, p's > .14. Accordingly, these factors were not included in the model as nuisance variables. Separate ANOVAs compared group (Low-Risk, High-Risk, and BSD) for each graph metric (clustering coefficient and path length), *Table 4*. There was no significant main effect of group on path length or clustering coefficient, p's > .34. There was no significant effect of age or psychiatric medication status on small world property, p's > .29, but there was a significant main effect of sex on small world property, $t(120) = 3.40$, $p = .018$. This sex difference was driven by women ($M = 2.54$, $SEM = .027$) who exhibited a higher correspondence to a small world neural network compared to men ($M = 2.46$, $SEM = .021$). Accordingly, sex was included as a nuisance variable

in the comparison of global small world property across groups. Small world property was evaluated in an ANCOVA that compared group (Low-Risk, High-Risk, and BSD) on small world property, accounting for sex as a nuisance variable. There were no significant main or interactive effects of group or sex on small world property, *p's* > .20.

Whole Brain Graph Theory Nodal Metrics. Graph metrics were also examined across each node (nodal metrics) and were corrected for with FDR correction because, unlike the theoretical subnetworks, there was no prior theoretical restriction to these analyses. No nodes were stable and significant with FDR correction across the biologically feasible range (20-30%) for either path length or clustering coefficient.

Whole Brain Theoretical Internetwork Hubs. Separate analyses evaluated potential relationships to the nodal graph metrics (path length and clustering coefficient) to age, sex, and psychiatric medication status, and were not significant, *p's*>.40. Nodal graph metrics (clustering coefficient and path length) were assessed across the high-risk design in critical internetwork hub regions (lOFC, mOFC, VS, amygdala) using repeated measure (right hemisphere and left hemisphere) general linear models, *Table 5*. In the whole brain network nodal graph metric analyses, there were no significant main of group or group by hemisphere interactive effects on the global path length in any of the hub regions, *p's* > .34. Similarly, there were no significant main of group or group by hemisphere interactive effects on the global clustering coefficient, *p's* > .38.

Whole Brain Structural Conclusions. I hypothesized that there would be whole brain differences consistent with reduced efficiency (increased path length and decreased clustering coefficient) in the BSD group, but the whole brain network appears intact structurally. This is

consistent with assumptions inherent to region of interest and pairwise connectivity literature, which assumes a largely intact network with specific sites of abnormalities.

Emotion Generation/Regulation Subnetwork Structure. In the following analyses subsection, structural connectivity graphs were calculated defining edges as the mean fractional anisotropy between nodes. Nodes were defined as set of theoretically relevant emotion generation/regulation 32 regions (16 regions by 2 hemispheres), including: VTA, VS, amygdala, insula, dACC, globus pallidus, mOFC, lOFC, dACC, dlPFC (FreeSurfer labels defined as: rostral middle frontal gyrus and caudal frontal gyrus), vlPFC (FreeSurfer labels defined as: frontal pole, pars orbitalis, pars triangularis, pars operculum), and dmPFC. The potential confounding effects of age, sex and psychiatric medication status were evaluated in separate analyses that examined their relationship to global graph metrics for these effects. Confounding variables were included in group analyses if they related to the graph metric. Global graph theory metrics were assessed in separate ANOVAs that compared group (Low-Risk, High-Risk, and BSD) in each graph metric (clustering coefficient and path length). Finally, nodal graph metrics (clustering coefficient and path length) evaluated whether there were differences for any node on these metrics; these analyses were corrected with simulated random graphs. In random graph correction 1,000 random graphs were simulated for each subject with a similar data dispersion and 1,000 bootstrapped samples were drawn from random graphs to generate a bootstrapped random group comparison. Nodal metrics were also assessed across the high-risk design (Low-Risk, High-Risk, and BSD) in critical internetwork hub regions (lOFC, mOFC, VS (FreeSurfer label defined as nucleus accumbens), amygdala) using repeated measure (left and right hemisphere) general linear models.

Emotion Generation/Regulation Subnetwork Graph Theory Global Metrics. Separate analyses evaluated potential relationships to the global graph metrics (clustering coefficient and path length) to age, sex, and psychiatric medication status. Clustering coefficient and path length global graph metrics were not related to age, sex, and psychiatric medication status, *p's* > .06. Accordingly, these factors were not included in the model as nuisance variables. Separate ANOVAs compared group (Low-Risk, High-Risk, and BSD) for each graph metric (clustering coefficient and path length), *Table 4*. There was no significant main or interactive effects of group and sex on path length in the emotion generation/regulation subnetwork, *p's* > .94. There was no significant main effect of group on clustering coefficient in the emotion generation/regulation subnetwork, *p's* > .91.

Emotion Generation/Regulation Subnetwork Graph Theory Nodal Metrics. In emotion generation/regulation regions there were significant group differences in path length in two nodes (right vlPFC and left amygdala) that were stable across the majority of the biologically feasible threshold, corrected using random simulated data correction. There was a significant group effect in the right vlPFC (frontal pole), $F(2,120) = 3.45$, $p = 0.004$, that was stable across the 20-30% threshold. Pairwise comparisons revealed that the BSD group had significantly greater path length in the vlPFC than both the Low-Risk, $t(70) = 2.60$, $p = .001$, $d = 1.02$, and High-Risk group, $t(82) = 1.26$, $p = .05$, $d = 0.52$. Also, a pairwise comparison revealed that the High-Risk group did not significantly differ in path length compared to the Low-Risk group, although there was a trend level effect, $t(90) = 1.38$, $p = .06$, $d = 0.52$, *Figure 1*. Follow-up analyses related path length in the right vlPFC to risk traits across the High-Risk and BSD groups. Separate bivariate correlations examined pathlength in the right vlPFC to BAS total

score and Sensitivity to Reward total score. There were no significant relationships between the emotion regulation/generation subnetwork in the right vlPFC and any markers of risk, *p's* > .12.

There was also a significant difference between groups in the left amygdala path length, $F(2,120)=2.86$, $p=0.02$, which was stable across 22-30% threshold. Pairwise comparisons revealed that the High-Risk group had significantly greater characteristic path length in the left amygdala than the BSD group, $t(82)=2.36$, $p=.006$, $d=0.76$ and a there was a trend level difference from the Low-Risk group, $t(70)=1.46$ $p=.07$, $d=0.51$. The BSD Group did not significantly differ from the Low-Risk group in terms of characteristic path length, $p=.21$, *Figure 2*. The group difference was driven by differences between the High-Risk and BSD groups, as a result the follow up analyses will treat path length in the frontal left amygdala as a potential corollary of BSD and examine the relationship of left amygdala to BSD features. Separate bivariate correlations found that emotion generation/regulation subnetwork path length in the left amygdala did not relate to age of onset or number of hypo/mania episodes within the BSD group, *p's*>.09.

Emotion Generation/Regulation Subnetwork Theoretical Internetwork Hub. Separate analyses evaluated potential relationships to the nodal graph metrics (path length and clustering coefficient) to age, sex, and psychiatric medication status, and were not significant, *p's*>.13. Nodal graph metrics (clustering coefficient and path length) were assessed across the high-risk design in critical internetwork hub regions (lOFC, mOFC, VS, amygdala) using repeated measure (right hemisphere and left hemisphere) general linear models, *Table 5*. In the emotion regulation theoretical subnetwork, there were no significant main or interactive effects of group on the emotion regulation path length in any of the internetwork hub regions, *p's* > .06. There

were no significant main or interactive effects of group on the emotion regulation clustering coefficient in any of the internetwork hub regions, *p's* > .35.

Emotion Generation/Regulation Subnetwork Structural Conclusion. As anticipated, restricting the network definition from a whole brain network to a theoretically relevant emotion generation/regulation network increased sensitivity to group differences in the high-risk design, albeit only in the nodal metric level. Emotion regulation regions (right vlPFC and left amygdala) showed increased path length in the BSD group compared to the Low-Risk group. The High-Risk group had and intermediary profile but did not significantly (p=.06) differ from the Low-Risk Group in the right vlPFC. This suggests that the increased vlPFC structural path length may be associated with the presence of a BSD diagnosis, but given the intermediate profile, between Low-Risk and BSD groups, it may also be a corollary of risk. However, the conclusion that vlPFC is a corollary of risk is made cautiously as right vlPFC did not relate to continuous measures of either risk or BSD symptoms. In the left amygdala (an emotion generation region) group differences were driven by differences between the High-Risk group and the BSD group, which suggests a corollary of BSD, but this interpretation is made cautiously as left amygdala path length did not relate continuously to features of BSD.

Reward Subnetwork Structure. In the following analyses subsection, reward regions structural connectivity graphs edges were defined as the mean fractional anisotropy between nodes. Nodes were defined as set of 12 regions (6 by 2 hemispheres), including: VTA, VS, amygdala, mOFC, lOFC, dACC). The potential confounding effects of age, sex and psychiatric medication status were evaluated in separate analyses that examined their relationship to graph metrics for these effects. Confounding variables were included in group analyses if they related

to the graph metric. Hub graph metrics were examined in separate repeated measure general linear models that compared group (Low-Risk, High-Risk, and BSD) on each graph metric (clustering coefficient and path length) for each hemisphere (left and right). Finally, nodal graph metrics (clustering coefficient and path length) evaluated whether there were differences for any node on these metrics; these analyses was corrected with simulated random graphs. In random graph correction 1,000 random graphs were simulated for each subject with a similar data dispersion and 1,000 bootstrapped samples were drawn from random graphs to generate a bootstrapped random group comparison. Nodal metrics were also assessed across the high-risk design in critical internetwork hub regions (lOFC, mOFC, VS (FreeSurfer label defined as nucleus accumbens), amygdala) using repeated measure general linear models.

Reward Subnetwork Global Graph Metrics. Separate analyses evaluated potential relationships to the global graph metrics (clustering coefficient and path length) to age, sex, and psychiatric medication status. Clustering coefficient and path length global graph metrics were not related to age or psychiatric medication status, *p's* > .10. Accordingly, these factors were not included in the model as nuisance variables. Clustering coefficient was significantly related to sex, $t(119) = 2.07$, $p = .04$, such that men ($M = 0.16$, $SEM = 0.008$) had slightly elevated path length compared to women ($M = 0.14$, $SEM = 0.008$). Path length in the reward network was significantly related to sex, $t(119) = 3.11$, $p =. 002$, such that women ($M = 5.16$, $SEM = 0.24$) had longer path lengths than men ($M = 4.16$, $SEM = 0.19$). As a result, sex was included in all subnetwork analyses. Separate ANCOVAs compared group (Low-Risk, High-Risk, and BSD) for each graph metric (clustering coefficient and path length) accounting for sex, *Table 4*. There was no significant main or interactive effect of groups and sex on path length in the reward

subnetwork, *p's* >. 30. There was no significant main or interactive effects of group and sex on clustering coefficient in the reward subnetwork, *p's* > .35.

Reward Subnetwork Nodal Graphs Metrics. In the reward subnetwork, graph metrics were also examined across each node (nodal metrics) and were corrected with simulated data as a null FWE, there was no prior theoretical restriction to these analyses. No nodes were stable and significant with FWE correction across the biologically feasible range (20-30%) for either path length or clustering coefficient.

Reward Subnetwork Theoretical Internetwork Hub Defined. Separate analyses evaluated potential relationships to the nodal graph metrics (path length and clustering coefficient) to age and psychiatric medication status, and were not significant, *p's*>.37. There was a significant effect of sex on clustering coefficient in the VS, $F(1,121) = 6.12$, $p = .015$, such that males had significantly higher clustering coefficient in the males ($M = .198$, $SEM = .019$) than females ($M = .134$, $SEM = .018$). Nodal graph metrics (clustering coefficient and path length) were assessed across the high-risk design in critical internetwork hub regions (lOFC, mOFC, VS, amygdala) using repeated measure (right hemisphere and left hemisphere) general linear models, *Table 5*. In the reward theoretical subnetwork, path length showed no significant main effect of group in any of the internetwork hub regions, *p's* > .42. Clustering coefficient had no significant of group on the mOFC, lOFC or amygdala, *p's* > .02.

In the VS, there were no significant main effects of group on clustering coefficient, *p's* > .07, *Table 7*. There was, however, a significant sex by group by hemisphere difference in clustering coefficient within the reward subnetwork, $F(2,120) = 5.00$, $p = .008$. Although, females ($M = .136$, $SEM = .019$) had significantly reduced clustering coefficient compared to

males (*M* = .199, *SEM* = 0.019) in the VS, *p* = .019, within sex there was no significant group or hemisphere differences among females. Among males, there were significant group differences within the right VS and left VS, and between hemispheres within the BSD group. In the right VS the Low-Risk group (*M* = .310, *SEM* =0.042) had significantly greater clustering coefficient than the BSD groups (*M* = .131, *SEM* = 0.049), but not the High-Risk (*M* = .155, *SEM* = 0.039).. In the left VS, the BSD group (*M* = .249, *SEM* = 0.049) had significantly elevated clustering coefficient compared to the Low-Risk (*M* = .2153, *SEM* = 0.043) but not the High-Risk group (*M* = .197, *SEM* = 0.040), *Figure 3.* Given that the High-Risk Group showed a non-significant intermediary phenotype in both hemispheres the follow up analyses examined whether right VS clustering coefficient is a correlate of risk. Accordingly, follow up analyses examined whether left and right VS Reward Network clustering coefficient is a correlate of risk in males. These analyses were restricted to males in the BSD and the High-Risk groups who were examined in a repeated measure general linear model comparing clustering coefficient relating the VS to the reward subnetwork to relevant risk metrics (BAS total score and Sensitivity to Reward total score). There were no significant relationships between clustering coefficient relating the VS to the reward subnetwork, *p's* > .07.

Reward Subnetwork Structural Conclusions. As anticipated, restricting the network definition from a whole brain network to a theoretically relevant reward network increased sensitivity to group differences in the high-risk design, but only in a theoretically defined internetwork hub region (VS). Theoretical internetwork hub analyses, however, revealed that structural connectivity of the VS within a reward neural network was abnormal among males with a BSD compared to the Low-Risk group. This VS effect varied by hemisphere such that the

structural clustering coefficient was significantly reduced in the left hemisphere and significantly increased in the right hemisphere. The High-Risk group did not significantly differ from either the Low-Risk or BSD group. Questions remain as to whether this sex by hemisphere by group interaction represents a correlate of risk or BSD. Additionally, it is not clear what is driving the sex difference.

Functional Graph Theory Results

This section examines functional network architecture in BSD behavioral high-risk design across three network definitions (whole brain, emotion generation/regulation, and reward) using global graph metrics, nodal graph metrics, and internetwork hub regions. The high-risk design allowed us to dissociate correlates of risk for BSD from correlates of BSD onset or progression. Correlates of risk for BSD were defined as significant differences that appear in both the High-Risk and the BSD groups. A correlate of risk may appear as an intermediate endophenotype between BSD and Low-Risk groups or where the High-Risk group does not differ from the BSD group. Correlates of the presence or progression of BSD were defined as significant differences that appear in the BSD group compared to either the Low-Risk or the High-Risk group, but critically correlates of BSD must distinguish between the BSD and the High-Risk groups. Furthermore, these graph theoretical analyses examined network architecture implicated in risk for BSD across three network definitions: (a) whole brain, (b) emotion generation/regulation subnetwork, and (c) reward subnetwork. These networks were examined in terms of global graph metrics, nodal graph metrics, and theoretical inter-network hubs. Finally, these two models of BSD (i.e., the reward hypersensitivity and emotion regulation models) have yet to be directly

examined as network structures; the following analyses are the first to examine these theories directly in terms of structural networks.

Functional Participant Demographics. Twenty individuals were excluded after visual quality check established that motion artifacts remained after correction. Among the twenty excluded the average framewise displacement pre-scrubbing was 4.06 (*StD* = 0.91), which was significantly different from the included sample (M=0.75; *SD*=0.44), $t(128) = 17.39$, $d = 2.59$, $p < .001$. The final analytic sample for the functional graph theory analyses was 111 (51% female) participants. This sample included 36 Low-Risk individuals, 46 High-Risk individuals, and 28 individuals with a bipolar spectrum diagnosis (BSD). The average age was 20.74 (*SD* = 1.93), and there was no significant group (Low-Risk, High-Risk, and BSD) difference within the final sample in age, $F(2,109) = 1.31$, $p = .27$. There was no significant difference in the ratio of sex to each group (Low-Risk, High-Risk, and BSD), $\chi^2(110) = 0.75$, $p = .69$. There were individuals taking psychiatric medications in each group (e.g., antidepressants, benzodiazepines) in each group: 5 in the Low-Risk group, 5 in the High-Risk group, and 4 in the BSD group. There was no significant difference in the incidence of medication use across these groups, $\chi^2(110) = 0.25$, $p = .88$.

Whole Brain Functional Network Analyses. In the following analyses subsection, global metrics of functional connectivity were extracted from the whole brain connectivity matrix where edges were defined as correlation of the spontaneous activity between nodes. The potential confounding effects of age, sex and psychiatric medication status were evaluated in separate analyses that examined their relationship to graph metrics for these effects. Confounding variables were included in group analyses if they related to the graph metric.

Global graph metrics were then evaluated in three separate analyses of variances (ANOVAs) comparing group (Low-Risk, High-Risk, and BSD) in each graph metric (clustering coefficient, path length, and small world property). Nodal graph metrics (clustering coefficient and path length) were also calculated for each node to evaluate whether there were differences in these graph metrics (clustering coefficient and path length) for any node. At the whole brain level, nodal analyses were exploratory corrected as such using FDR correction. Nodal metrics were also assessed across the high-risk design in critical internetwork hub regions [lOFC, mOFC, VS (FreeSurfer label defined as nucleus accumbens), amygdala] using repeated measure (right and left hemisphere) general linear models.

Whole Brain Graph Theory Global Metrics. Separate analyses evaluated potential relationships to the global graph metrics (clustering coefficient, path length, and small world property) to age, sex, and psychiatric medication status. There was no significant relationship between small world property or clustering coefficient and any of the confounding variables, *p's* > .18. There was no significant relationship between path length and age or psychiatric medication status, *p's*>.19. There was, however, a significant sex difference in path length, $t(109) = 2.51$, $p = .014$, such that females ($M = 10.85$, $SEM = .061$) had greater path length than males ($M = 10.65$, $SEM = .049$). Separate ANOVAs compared global graph metrics (small world property, clustering coefficient and path length) across Low-Risk, High-Risk and BSD groups, *Table 4.* These analyses found no main or interactive effects of group on small world property, clustering coefficient, or path length, *p's* > .85.

Whole Brain Graph Theory Nodal Metrics. Graph metrics were also examined across each node (nodal metrics) and were corrected for with FDR correction because, unlike the

theoretical subnetworks, there was no prior theoretical restriction to these analyses. No nodes were stable and significant with FDR correction across the biologically feasible range (20-30%) for either path length or clustering coefficient.

Whole Brain Theoretical Internetwork Hubs. Separate analyses evaluated potential relationships to the nodal graph metrics (path length and clustering coefficient) to age, sex, and psychiatric medication status, and were not significant, *p's*>.08. Nodal graph metrics (clustering coefficient and path length) were assessed across the high-risk design in critical internetwork hub regions (lOFC, mOFC, VS, amygdala) using repeated measure (right hemisphere and left hemisphere) general linear models, *Table 5*. No other hub region (mOFC, VS, or amygdala) showed a significant group difference in clustering coefficient, *p's* > .22. There were also no significant relationships between path lengths in any of the hub regions at a whole brain network, *p's* > .017.

Whole Brain Functional Conclusions. I hypothesized that there would be whole brain differences consistent with reduced efficiency (increased path length and decreased clustering coefficient) in the BSD group, but the whole brain network is largely intact functionally.

Emotion Generation/Regulation Subnetwork Structure Analyses. In the following analyses subsection, resting state functional connectivity graphs were calculated where edges were defined as correlation of the spontaneous activity between nodes. Nodes were defined as a set of theoretically relevant emotion generation/regulation 32 regions (16 regions by 2 hemispheres), including: VTA (FreeSurfer label defined as nucleus accumbens), VS, amygdala, insula, dACC, globus pallidus, mOFC, lOFC, dACC, dlPFC (FreeSurfer labels defined: rostral middle frontal gyrus and caudal frontal gyrus), vlPFC (FreeSurfer labels defined: frontal pole,

pars orbitalis, pars triangularis, pars operculum), and dmPFC. The potential confounding effects of age, sex and psychiatric medication status were evaluated in separate analyses that examined their relationship to global graph metrics for these effects. Confounding variables were included in group analyses if they related to the graph metric. Global graph theory metrics were assessed in separate ANOVAs compared group (Low-Risk, High-Risk, and BSD) in each graph metric (clustering coefficient and path length). Finally, nodal graph metrics (clustering coefficient and path length) evaluated whether there were differences for any node on these metrics; these analyses was corrected with simulated random graphs. In random graph correction 1,000 random graphs were simulated for each subject with a similar data dispersion and 1,000 bootstrapped samples were drawn from random graphs to generate a bootstrapped random group comparison. Nodal metrics were also assessed across the high-risk design in critical internetwork hub regions (lOFC, mOFC, VS, amygdala) using repeated measure general linear models.

Emotion Generation/Regulation Subnetwork Graph Theory Global Metrics. Separate analyses evaluated potential relationships to the global graph metrics (clustering coefficient and path length) to age, sex, and psychiatric medication status. In the emotion generation/regulation subnetwork, there was a significant relationship between clustering coefficient and sex, $t(110) = 2.22$, $p = .028$. Females ($M = .23$, $SEM = .004$) showed significantly reduced clustering coefficient compared to males ($M = .24$, $SEM = .004$). Similarly women ($M = 4.73$, $SEM = .078$) showed a significantly elevated path length compared to men ($M = 4.50$, $SEM = .074$) in the emotion generation/regulation subnetwork, $t(110) = 2.15$, $p = .04$. Accordingly, all emotion subnetwork graph evaluations accounted for sex differences as a nuisance variable. Separate ANCOVAs examined the main effect of group on global graph metrics (clustering coefficient

and path length) accounting for the difference in sex, *Table 4*. There was no significant main effect of group on clustering coefficient or path length in the reward subnetwork, *p's* > .26.

Emotion Generation/Regulation Subnetwork Graph Theory Nodal Metrics. Nodal metrics (path length and clustering coefficient) were examined across the biologically feasible threshold (20-30%) and corrected with simulated data. In the clustering coefficient nodal comparison there was a significant group difference in the left dlPFC (FreeSurfer label defined as rostral middle frontal gyrus), $F(2,109) = 3.16$, $p = .001$, that was stable from 20-26% threshold. The Low-Risk group had significantly higher clustering coefficient in the dlPFC compared to both the High-Risk group, $p = .003$, and the BSD group, $p < .001$. There was no significant difference between the BSD and High-Risk groups, $p = .47$. Separate correlations evaluated the relationship of significant nodal findings and the risk metrics (BAS and SR) in the BSD and High-Risk groups. There were no significant relationships between clustering coefficient for the left dlPFC in the emotion generation/regulation subnetwork and any risk metric, *p's* > .50, *Figure 5*.

There was a significant group difference in path length in the left dACC, $F(2,109) = 4.88$, $p = .013$, that was stable across the entire 20-30% range. There was a marginally significant difference between the Low-Risk group and the High-Risk group, $p = .050$, $d = .635$, such that the High-Risk group had a greater path length than the Low-Risk Group. The BSD group also had a significantly greater path length than the Low-Risk group, $p = .005$, $d = 1.179$. There was no significant difference between the High-Risk and Low-Risk group, $p = .09$, $d = 0.54$. This pattern of results in the left dACC appeared to be a correlate of risk for BSD, as such follow up analyses compared path length in left dACC to continuous risk variables (BAS and SR). There

were no significant relationships between path length for the left dACC in the emotion generation/regulation subnetwork and any risk metric, *p's* > .29, *Figure 6*.

Emotion Generation/Regulation Subnetwork Theoretical Internetwork Hub. Separate analyses evaluated potential relationships to the nodal graph metrics (path length and clustering coefficient) to age, sex, and psychiatric medication status, and were not significant, *p's*>.07. Nodal graph metrics (clustering coefficient and path length) were assessed across the high-risk design in critical internetwork hub regions (lOFC, mOFC, VS, amygdala) using repeated measure (right hemisphere and left hemisphere) general linear models, *Table 5*. There were no main or interactive group effects of clustering coefficient in any of the theoretical network hubs (lOFC, mOFC, VS, or Amygdala), *p* > .15. There were also no main or interactive group effects of path length in any of the theoretical network hubs, p's > .06.

Emotion Generation/Regulation Subnetwork Functional Conclusions. As anticipated, restricting the network definition from a whole brain network to a theoretically relevant emotion generation/regulation network increased sensitivity to group differences in the high-risk design, albeit only at the nodal metric level. Emotion regulation regions (left dlPFC and left dACC) were significantly different (increased path length and decreased clustering coefficient, respectively) in the BSD and High-Risk groups compared to the Low-Risk group. The High-Risk group had and intermediary profile in both regions, which significantly differing from Low-Risk Group in the both the dACC and dlPFC. This suggest that, functionally, the dlPFC clustering coefficient and dACC path length are correlates of risk for BSD. However, these interpretations are made cautiously as path length did not relate to continuous measures of either risk or BSD symptoms.

Reward Subnetwork Structure Analyses. In the following analyses subsection, the reward regions functional connectivity graphs edges were defined as correlation of the spontaneous activity between nodes. Nodes were defined as a set of 12 theoretically defined regions (6 by 2 hemispheres), including: VTA, VS, amygdala, mOFC, lOFC, dACC). The potential confounding effects of age, sex and psychiatric medication status were evaluated in separate analyses that examined their relationship to global graph metrics for these effects. Confounding variables were included in group analyses if they related to the graph metric. Global graph metrics were examined in separate ANOVAs that compared group (Low-Risk, High-Risk, and BSD) on each graph metric (clustering coefficient and path length). Finally, nodal graph metrics (clustering coefficient and path length) evaluated whether there were differences for any node on these metrics; these analyses were corrected with simulated random graphs. In random graph correction 1,000 random graphs were simulated for each subject with a similar data dispersion and 1,000 bootstrapped samples were drawn from random graphs to generate a bootstrapped random group comparison. Nodal metrics were also assessed across the high-risk design in critical internetwork hub regions (lOFC, mOFC, VS, amygdala) using repeated measure (left hemisphere, right hemisphere) general linear models.

Reward Subnetwork Global Graph Metrics. Separate analyses evaluated potential relationships to the global graph metrics (clustering coefficient and path length) to age, sex, and psychiatric medication status. Clustering coefficient and path length global graph metrics were not related to age, sex, and psychiatric medication status, p's > .16. Accordingly, these factors were not included in the model as nuisance variables. Separate ANOVAs compared group (Low-Risk, High-Risk, and BSD) for each graph metric (clustering coefficient and path length), *Table*

4. There was no significant main effect of group on clustering coefficient or path length in the reward subnetwork, *p's* > .61.

Reward Subnetwork Nodal Graph Metrics. In the reward subnetwork, graph metrics were also examined across each node (nodal metrics) and were corrected with simulated data as a null FWE, there was no prior theoretical restriction to these analyses. No nodes were stable and significant with FWE correction across the biologically feasible range (20-30%) for either path length or clustering coefficient.

Reward Subnetwork Theoretical Internetwork Hub. Separate analyses evaluated potential relationships to the nodal graph metrics (path length and clustering coefficient) to age, sex, and psychiatric medication status, and were not significant, *p's*>.06. Nodal graph metrics (clustering coefficient and path length) were assessed across the high-risk design in critical internetwork hub regions (lOFC, mOFC, VS, amygdala) using repeated measure (right hemisphere and left hemisphere) general linear models, *Table 5*. There were no main or interactive group effects of clustering coefficient in any of the theoretical network hubs (lOFC, mOFC, VS, or Amygdala), *p* > .09. There were no main or interactive group effects of path length in any of the theoretical network hubs (lOFC, mOFC, VS, or Amygdala), *p* > .20.

Reward Subnetwork Functional Conclusions. Contrary to my hypothesis, restricting the network definition from a whole brain network to a theoretically relevant reward network did not increase sensitivity to functional group differences in the high-risk design. These analyses suggest that the reward network is intact functionally across the bipolar risk spectrum.

Discussion

Decreased network efficiency in emotion regulation regions was a corollary of risk for BSD both functionally and structurally. In contrast, structural network abnormalities in an emotion generation region was a corollary of the presence or progression of BSD. In the following section the broader implications and details of these findings are considered. First, I review the primary and theoretical aims of this paper. Next, I reiterate my hypothesis prior to analyses. Then, I summarize the findings based on the analyses. Finally, I discuss the current findings in the context of current literature, potential theoretical implications, and the broader impacts of the study.

Current Study Aims. This study examined structural and functional network architecture in a behavioral high-risk design, which dissociated correlates of risk for BSD from correlates of BSD. Network architecture was in risk and clinical groups were compared in three network definitions: whole brain network, theoretically defined emotion generation/regulation subnetwork, and theoretically defined reward subnetwork. Within each of these network definitions, graph metrics were calculated as global metrics, nodal metrics, and theoretical internetwork hub regions. Global analyses examined if the networks were largely intact, an assumption made inherently in region of interest and pairwise connectivity models. Taken together these analyses were also able to examine whether restricting network definitions, from a whole brain network to theoretically defined subnetworks, improved sensitivity to BSD relevant network differences. Additionally, the theoretical subnetwork analyses directly examined two neurobiological models of BSD (i.e., the emotion regulation model and the reward hypersensitivity model). While the literature supporting these models has relied on partial

information afforded by region of interest and pairwise connectivity approaches, this project directly examined the network architecture associated with BSD risk or the presence of a BSD diagnosis.

Current Study Hypotheses. Prior to analyses, I proposed a single set of hypotheses that I expected to converge across structural and functional graph network analyses. I hypothesized that BSD would be associated with global differences in functional and structural neural network architecture in the whole brain network. In the emotion generation/regulation subnetworks, I expected that BSD would be associated with reduced efficiency in emotion regulation regions and increased efficiency in emotion generation regions (consistent with emotion dysregulation models of BSD). In the reward subnetwork, I expected that there would be greater efficiency associated with risk for BSD (consistent with the reward hypersensitivity model of BSD). I, also, expected that restricting network definitions to theoretical subnetworks increased sensitivity to network differences in BSD. Similarly, I excepted that examining theoretical internetwork hubs, where emotion generation and emotion regulation networks converge, would increase sensitivity to potential structural and functional brain networks. Finally, I expected structural and functional network architecture to largely converge.

Current Study Findings. Risk for BSD related to decreased network efficiency in emotion regulation regions, both functionally and structurally. Corollaries of the presence and progression of BSD related to structural network abnormalities in an emotion generation region. In whole brain analyses, neither the High-Risk group nor the BSD group demonstrated distinct global metric network architecture for whole brain, emotion generation/regulation, or reward network levels. This finding was not consistent with my hypothesis, based early work by Leow

et al. (2013). However, this finding was consistent with recent literature that also found no difference in global metrics associated with BSD (Collin, Scholtens, Kahn, Hillegers, & van den Heuvel, 2017; Forde et al., 2016; Spielberg et al., 2016; Wang et al., 2018). While the neural network structure appears intact globally across the bipolar spectrum, critical nodal differences became apparent when networks were defined in terms of theoretically relevant emotion regulation and reward networks.

Restricting graph networks (from whole brain to emotion generation/regulation and reward subnetworks) increased sensitivity to nodal differences between the groups within theoretical subnetworks as expected. In emotion generation/regulation subnetwork analyses, reduced network effectiveness (increased path length/decreased clustering coefficient) in emotion regulation regions (right vlPFC, left dACC, left dlPFC) was a correlate of risk for BSD in both structural and functional networks. In emotion generation regions, structural networks found abnormalities in the left amygdala was a corollary of BSD within an emotion generation/regulation network. In the reward subnetwork, males with a BSD showed with aberrant clustering coefficient between the VS in structural internetwork hub analyses consistent with my hypothesis. These structural and functional network findings did not converge topographically, but findings did provide theoretically consistent results. Both functional and structural networks related emotion regulation to risk for BSD, while emotion generation nodes distinguished between the High-Risk and BSD groups in structural networks only.

In summary, global metrics suggested intact networks. In contrast nodal metrics found group differences that relate to risk for BSD in theoretically defined subnetworks. The nodal findings largely suggest that structural and functional network abnormalities in emotion

regulation regions were correlates of risk for BSD and that structural network abnormalities in emotion generation regions may be a correlate of BSD. Finally, internetwork hub analyses found structural network differences in the VS that varied by sex and hemisphere. These findings are discussed below in terms of the current literature, theoretical implications, and future directions.

Whole Brain Network and Global Graph Metrics. Whole brain analyses and global graph metrics suggest that neural networks are intact along the bipolar spectrum. While I hypothesized that networks would vary along the bipolar spectrum, consistent with Leow et al. (2013), there were no significant differences at the whole brain level or in any global metric analyses of the emotion regulation or reward subnetworks. This finding is contrary to early evidence that found group differences in structure at a global graph metric level (Leow et al., 2013). However, the analyses conducted by Leow et al. (2013) were largely comparing interhemispheric differences in global graph metrics, which may drive the global differences observed in that study and explain why there were no significant global differences in the current study. Recent literature on BSD had found that global graph metrics are largely intact across the bipolar spectrum, and that differences can be detected on a nodal level in these metrics (Collin, Scholtens, Kahn, Hillegers, & van den Heuvel, 2017; Forde et al., 2016; Roberts et al., 2016; Spielberg et al., 2016; Wang et al., 2018). Therefore, the current study found converging evidence of a largely intact network in global graph metrics, but that nodal graph metrics reveal differences in BSD network structure.

Converging evidence of intact global graph metrics and whole brain network structure provides support for the network assumptions inherent in BSD region of interest and pairwise connectivity literature. As stated in previous sections, BSD literature examines neural regions in

isolation of the network in which they are embedded or in terms of pairwise connectivity (Damme, Young, & Nusslock, 2017; Nusslock et al., 2012). This region of interest and pairwise connectivity approach assumes an overall intact network but does not directly examine this possibility. As a result, previous research is not able to examine whether observed correlates in BSD were the result of abnormalities within a node, a balance of connectivity to a node, or the downstream effect of larger network disruption. The current study, however, used graph theory analyses to directly examine the intact network assumption. The null global metric results provided evidence that BSD networks may be globally intact. A globally intact network suggests that BSD abnormalities are less likely to be the downstream result of a largely disrupted network. However, region of interest and pairwise analyses also assume that relevant neural network differences along a bipolar spectrum are largely driven by differences within a single region or pairs of regions. This latter assumption is challenged by nodal graph metric findings.

While it is true that neural networks appear largely intact across the bipolar spectrum, there are distinct nodal graph network features that vary along the bipolar spectrum. Nodal graph network differences do not imply that there are differences only within a region (supporting a region of interest approach) or in specific critical pairs (supporting a pairwise connectivity approach). Instead, nodal graph metric differences highlight the importance of the relevant network context for a given node. A significant nodal finding suggests not only that a node is the site of differences in connectivity but that the site has distinct connectivity in the context of a multi-region network. As such, examining the region in isolation or in the context of pairwise connectivity may provide incomplete information regarding aberrant connectivity of that node

within a network. Thus, while these findings provide evidence of an intact network, they also highlight the value of examining single nodes in the context of a theoretical neural network.

Theoretical Subnetworks. Examining nodal graph metrics in terms of theoretical subnetworks increased the sensitivity to group differences. This result is consistent with our hypothesis and with other studies that have found no differences at a global level, but restricting network definitions increased sensitivity to group differences in BSD (GadElkarim et al., 2014; Manelis et al., 2016; Wang et al., 2018). The current study defined theoretically relevant emotion generation/regulation and reward subnetworks which increased sensitivity to group differences associated with BSD in emotion generation/regulation and reward subnetworks. The results of each theoretical network are discussed below.

Emotion Generation/Regulation Subnetwork. Emotion generation/regulation subnetwork analyses found an inefficient network structure (increased nodal path length/decreased clustering coefficient) in emotion regulation nodes both structurally (right vlPFC) and functionally (left dACC and left dlPFC). Emotion regulation nodes were correlates of risk for BSD distinguishing the Low-Risk from the High-Risk (though only at a trend level in vlPFC). These nodal BSD abnormalities appeared only in the structural (vlPFC) or functional (dlPFC, dACC) graphs. Notably, the only emotion generation node identified (left amygdala) was a corollary of the presence or progression of BSD (distinguished between the BSD and High-Risk group) in an emotion generation/regulation network. Collectively, these findings suggest that risk for BSD is associated with poorer network efficiency (increased path length and decreased clustering coefficient) in emotion regulation regions, consistent with a "top-down" regulation hypothesis emotion dysregulation neurobiological model of BSD. Additionally, the

emotion generation region (left amygdala) abnormalities network is consistent with a "bottom up" emotion dysregulation hypothesis (Phillips, Ladouceur, & Drevets, 2008). Taken together, risk may be conferred by a "top down" reduction in emotion regulation, while BSD onset and progression maybe related to structural abnormalities in the emotion generation networks.

Emotion regulation network structure were corollaries of risk for BSD and may provide a good target for psychosocial or neuromodulatory intervention. Neurodevelopmental studies of emotion regulation regions found a large window of development in emotion regulation networks (age 10.5-25; Mills et al., 2016, Giedd, Raznahan, Mills, & Lenroot, 2012) near the typical BSD onset (ages 17-25; Bellivier et al., 2003; Paus, Keshavan, & Giedd, 2008). The co-occurrence of network development and BSD onset may suggest that these network abnormalities relate to the onset of BSD. If so, there may a development window of time where these networks are still developing prior to the onset of BSD where emotion regulation may be improved through psychosocial or neuromodulatory intervention to prevent BSD onset or progression (Mills & Tamnes, 2014). Prospective, longitudinal work is needed to confirm whether the emotion regulation functional and structural networks differences relate to BSD onset during this period. Additionally, future studies should examine whether psychosocial or neuromodulatory intervention are able to successfully modulate structural and functional development in emotion regulation networks.

Reward Subnetwork. Restricting the network definition to the reward subnetwork did not confer additional sensitivity to corollaries of risk in BSD. However, theoretic internetwork hub analyses revealed that a three-way interaction, a sex by hemisphere by group interaction, at VS node in a reward network was a correlate of risk for BSD, distinguishing between Low-Risk and

BSD groups but not the High-Risk group. This finding is consistent with past BSD risk literature suggests that the elevated structural connectivity of the VS to reward related regions predicts elevated risk for BSD (Damme, Young & Nusslock, 2017). This three-way interaction suggested that aberrant structural connectivity (clustering coefficient) for the VS within the reward subnetwork was correlate of risk for BSD among males. Among males, the direction of this VS hub effect varied by hemisphere, such that BSD was associated with a significantly elevated clustering coefficient in the left VS and significantly reduced in the right VS, compared to the Low-Risk group. The High-Risk group, however, did not significantly differ from the Low-Risk or BSD groups in either hemisphere, displaying an intermediary clustering coefficient. The High-Risk group was significantly lower than the Low-Risk group in the right VS, which may suggest that the clustering coefficient is a correlate of risk for males. In contrast, the left VS did not differ in males between males in the High-Risk and Low-Risk group, which leaves ambiguity as to whether this effect is a correlate of risk for BSD or a related to the presence or progression of BSD.

This VS sex by group by hemisphere interaction has three nuances to consider in the interpretation of the findings: the difference between hemispheres, the intermediary profile of High-Risk group, and the difference between sexes. Structural clustering coefficient in the VS also varied by hemisphere. While this hemisphere effect was not expected based on neuroanatomical models of BSD, there is BSD literature that suggests hemispheric differences in structural graph theory analyses (Leow et al., 2013). Particularly, Loew et al. (2013) suggested that hemispheric differences in structural frontal-limbic networks are driven by reduced corpus collosum volume. While Leow et al. (2013) provides a potential explanation of interhemispheric

differences, more research is needed to examine this possibility. Findings of hemispheric differences emphasizes the need for future studies to examine graph networks both within and across hemispheres.

The intermediary profile in the High-Risk group for the left VS suggests a few possibilities. First, males at High-Risk for BSD may truly display a higher structural clustering coefficient in the left VS that are intermediary between those with a BSD and those at low risk for the disorder. Second, these findings may reflect potential heterogeneity of the High-Risk group. Namely, our High-Risk group may be a mixture of individuals who will never go on to develop a BSD and individuals who are truly at risk and who will go on to develop a BSD. Heterogeneity in the High-Risk group may obscure the relation between elevated structural clustering coefficient in the left VS and BSD vulnerability. Finally, structural clustering coefficient in the left VS may become more abnormal upon approaching the first mood episode, which also may explain why the High-Risk group did not yet significantly differ from either Low-Risk or BSD groups. These possibilities emphasize the need for longitudinal studies to prospectively predict conversion from the High-Risk for BSD group to the BSD group.

Finally, it is also important to consider the implications of this sex difference. This internetwork hub effect may reflect a sincere sex difference, but it is important for future studies to consider sex differences in symptomatology. In particular, men with a BSD tend to present with more mania, while women report high levels of depression (Goodwin & Jamison, 2007; Saunders et al., 2015), and so it is possible that mania symptoms are driving sex differences in structural clustering coefficient in the VS. Furthermore, past structural connectivity work suggests that elevated structural connectivity in the VS is associated with increased levels of

hypo/mania (Damme, Young, & Nusslock, 2017). This relationship between VS structural connectivity and hypo/mania underscores the possibility that the observed sex difference in structural connectivity in the VS may be mediated by level of mania. Unfortunately, the current study is underpowered to examine the relationship of mania to VS clustering coefficient within males with a BSD. Future studies should examine sex differences in symptomatology may relate to structural clustering coefficient in the VS.

While the current findings do not provide clear evidence in support of the reward hypersensitivity model, there are important potential implications of the null results. Notably, past evidence supporting the reward hypersensitivity model is based on behavior or task-related neural activity (Alloy & Nusslock, 2018; Nusslock, Young, & Damme, 2014 for review). Given that past emphasis on task-related neural activity, it is possible that reward hypersensitivity is not a stable network difference, which would observable in structural or resting-state functional networks. Instead reward hypersensitivity may be a stimulus specific network reactivity that is only observable in the presence of reward stimuli.

A stimulus specific reward network difference is consistent with Manelis et al. (2016) who found reward-related functional network differences during a task. The task-related network differences in isolation may be the driven by stable network differences driven by stable differences in resting-state functional or structural networks. However, the current null resting-state functional and structural network findings suggests that reward-related functional network differences are stimulus specific rather than a stable network difference. Rather, collectively these findings may suggest that reward hypersensitivity in BSD is related to a dynamic, stimulus specific functional response, rather than converging task-based, resting-state, and structural

analyses. Another possibility is that the emotion regulation/generation networks abnormalities result in the abnormal reward-related task activity in the presence of reward stimuli (Manelis et al., 2016). Future studies should examine whether nodal emotion regulation/generation network differences (observed in structural and resting-state functional networks) relate to task-based functional differences in reward networks.

Structural and Functional Network Convergence. If structural and functional networks reflected multiple measures of a single underlying network structure (Deco et al., 2013; Deco, Jirsa, & McIntosh, 2011; Poldrack et al., 2015), then structural and functional data should converge to describe the same abnormalities in the network structure. However, as discussed in the introduction, structural and functional networks describe distinct biological features that may provide unique insight regarding the underlying neural network. Structural connectivity reflects features of white matter tissue, which develops in early adulthood and is relatively stable until late adulthood (Seehaus et al., 2015). In contrast, resting state functional connectivity reflects consistent (Poldrack et al., 2015), but dynamic configurations of cognitive networks (Collin, Scholtens, Kahn, Hillegers, & van den Heuvel, 2017). Given these differences between structural and functional metrics, it is possible that functional and structural graph metrics could reflect distinct features of the underlying neural networks. In fact, recent studies suggest that functional and structural coupling may reflect a reduced capacity for dynamic functional reconfiguration in neural circuits. The capacity for dynamic functional reconfiguration may reflect cognitive adaptability beyond anatomical restrictions (Collin, Scholtens, Kahn, Hillegers, & van den Heuvel, 2017; van den Heuvel et al., 2013). Considering this research, it is unsurprising that structural and functional connectivity did not converge topographically as function is not

restricted to structure. Instead, both structural and functional nodal metrics provided theoretically consistent and complimentary evidence that decreased network effectiveness (increased path length and reduced clustering coefficient) in emotion regulation regions was a correlate of risk for BSD in nodal graph metric analyses.

Recent work examining functional-structural network coupling have several implications for the current study (Collin, Scholtens, Kahn, Hillegers, & van den Heuvel, 2017; van den Heuvel et al., 2013). First, the complimentary findings of emotion regulation in distinct areas, may actually reflect that functional emotion generation network structure is dynamically compensating for the early occurring and stable structural network abnormality in both emotion regulation and emotion generation regions (Collin, Scholtens, Kahn, Hillegers, & van den Heuvel, 2017; van den Heuvel et al., 2013). Future research should longitudinally examine functional and structural network development to determine whether the abnormalities in structural networks precede and predict the network changes in function. Second, emotion generation nodal network abnormalities (left amygdala and bilateral VS) were only observed in structural networks, not functional networks. This selectivity of emotion generation abnormalities to structural networks may suggest that the improved network efficiency in emotion generation network nodes do not relate to a corresponding function network change. Alternatively, emotion generation regions may not show a dynamic cognitive compensation for structural differences at rest, but there may be dynamic functional network differences in the presence of emotional stimuli (Manelis et al., 2016). Future research should examine whether the emotion generation correlates of BSD observed structurally, impact the functional network dynamics during emotion relevant tasks.

Current Study Conclusions. In conclusion, whole brain networks and global metrics suggest that neural networks are largely intact. Examining subnetworks increased sensitivity to differences across a bipolar risk spectrum. Differences between groups were found only in nodal analyses within theoretically defined subnetworks. In the emotion generation/regulation subnetwork, both structural and functional connectivity suggests that increased path length in emotion regulation regions may reflect risk for BSD. Although structural and functional data did not topographically converge, they did provide complimentary theoretical evidence in the emotion generation/regulation subnetwork analyses. Additionally, a structural connectivity difference in an emotion generation node (left amygdala) was a corollary of BSD. Collectively, these findings support that functional and structural connectivity in emotion regulation nodes may be a correlate of risk for BSD while abnormal structural connectivity in an emotion generation node (left amygdala) may be a correlate of BSD. In the reward subnetwork, abnormal structural connectivity to reward network regions in the VS was a correlate of risk among men. Collectively, these results provided critical theoretical insight into intact network assumptions, theoretical models of BSD, corollaries of risk, and corollaries of BSD presence and progression. Additionally, this work suggests that emotion regulation networks may be a critical therapeutic target for future research to mitigate risk for BSD.

References

Alloy, L. B., Abramson, L. Y., Walshaw, P. D., Cogswell, A., Grandin, L. D., Hughes, M. E., Iacoviello, B. M., Whitehouse, W. G., Urosevic, S., Nusslock, R., & Hogan, M. E. (2008). Behavioral Approach System and Behavioral Inhibition System sensitivities and bipolar spectrum disorders: prospective prediction of bipolar mood episodes. *Bipolar Disorder*, *10*(2), 310–322.

Alloy, L. B., Abramson, L. Y., Whitehouse, W. G., Hogan, M. E., Panzarella, C., & Rose, D. T. (2006). Prospective incidence of first onsets and recurrences of depression in individuals at high and low cognitive risk for depression. *Journal of Abnormal Psychology*, *115*(1), 145–156.

Alloy, L. B., Bender, R. E., Whitehouse, W. G., Wagner, C. A., Liu, R. T., Grant, D. A., Abramson, L. Y. (2012a). High Behavioral Approach System (BAS) sensitivity, reward responsiveness, and goal-striving predict first onset of bipolar spectrum disorders: a prospective behavioral high-risk design. *Journal of Abnormal Psychology*, *121*(2), 339–351.

Alloy, L. B., Urošević, S., Abramson, L. Y., Jager-Hyman, S., Nusslock, R., Whitehouse, W. G., & Hogan, M. (2012b). Progression along the bipolar spectrum: A longitudinal study of predictors of conversion from bipolar spectrum conditions to bipolar I and II disorders. *Journal of Abnormal Psychology*, *121*(1), 16.

Alloy, L. B., & Nusslock, R. (2018). Reward-related cognitive vulnerability to bipolar spectrum disorders. *World Psychiatry*, *17*(1), 102-103.

Alloy, L. B., Nusslock, R., & Boland, E. M. (2015). The development and course of bipolar spectrum disorders: an integrated reward and circadian rhythm dysregulation model. *Annual*

Review Clinical Psychology, *11*, 213–250.

Alloy, L. B., Urosevic, S., Abramson, L. Y., Jager-Hyman, S., Nusslock, R., Whitehouse, W. G., & Hogan, M. (2012). Progression along the bipolar spectrum: a longitudinal study of predictors of conversion from bipolar spectrum conditions to bipolar I and II disorders. *Journal of Abnormal Psychology*, *121*(1), 16–27.

Andrews-Hanna, J. R., Reidler, J. S., Sepulcre, J., Poulin, R., & Buckner, R. L. (2010). Functional-Anatomic Fractionation of the Brain's Default Network. *Neuron*, *65*(4), 550–562.

Angst, F., Stassen, H. H., Clayton, P. J., & Angst, J. (2002). Mortality of patients with mood disorders: follow-up over 34-38 years. *Journal of Affective Disorders*, *68*(2–3), 167–181.

Barnett, J. H., & Smoller, J. W. (2009). The genetics of bipolar disorder. *Neuroscience*, *164*(1), 331-343.

Bassett, D. S., & Sporns, O. (2017). Network neuroscience. *Nature Neuroscience*, *20*(3), 353–364.

Bellivier, F., Golmard, J. L., Rietschel, M., Schulze, T. G., Malafosse, A., & Preisig, M. (2003) Age at onset in bipolar I affective disorder: further evidence for three subgroups. *American Journal of Psychiatry*, *160*(5), 999-1001.

Birmaher, B., Axelson, D., Goldstein, B., Strober, M., Gill, M. K., Hunt, J., Houck, P., Ha, W., Iyengar, S., Kim, E., Yen, S., Hower, H., Esposito-Smythers, C., Goldstein, T., Ryan, N., & Keller, M. (2009). Four-year longitudinal course of children and adolescents with bipolar spectrum disorders: The Course and Outcome of Bipolar Youth (COBY) study. *American Journal of Psychiatry*, *166*(7), 795–804.

Biswal, B., Zerrin Yetkin, F., Haughton, V. M., & Hyde, J. S. (1995). Functional connectivity in the motor cortex of resting human brain using echo-planar MRI. *Magnetic Resonance in Medicine*, *34*(4), 537–541.

Braun, U., Plichta, M. M., Esslinger, C., Sauer, C., Haddad, L., Grimm, O., Mier, D., Mohnke, S., Heinz, A., Erk, S., Walter, H., Seiferth, N., Kirsch, P., & Meyer-Lindenberg, A. (2012). Test-retest reliability of resting-state connectivity network characteristics using fMRI and graph theoretical measures. *NeuroImage*, *59*(2), 1404–1412.

Brown, J. A. (2018). UMPC [Software]. Available from https://github.com/jbrown81/umcp.

Bullmore, E., & Sporns, O. (2009). Complex brain networks: graph theoretical analysis of structural and functional systems. *Nature Reviews Neuroscience, 10*, 186-198.

Bullmore, E., & Sporns, O. (2012). The economy of brain network organization, *Nature Reviews Neuroscience, 13*, 336–349.

Carver, C. S., Johnson, S. L., Joormann, J., Kim, Y., & Nam, J. Y. (2011). Serotonin transporter polymorphism interacts with childhood adversity to predict aspects of impulsivity. *Psychological Science*, *22*(5), 589–595.

Carver, C. S., & White, T. L. (1994). Behavioral inhibition, behavioral activation, and affective responses to impending reward and punishment: The BIS/BAS Scales. *Journal of Personality and Social Psychology*, *67*(2), 319–333.

Cassano, G. B., Dell'Osso, L., Frank, E., Miniati, M., Fagiolini, A., Shear, K., Pini, S., & Maser, J. (1999). The bipolar spectrum: a clinical reality in search of diagnostic criteria and an assessment methodology. *Journal of Affective Disorders*, *54*(3), 319–328.

Collin, G., van den Heuvel, M. P., Abramovic, L., Vreeker, A., de Reus, M. A., van Haren, N. E.

M., Boks, M. P., Ophoff, R. A., & Kahn, R. S. (2016). Brain network analysis reveals affected connectome structure in bipolar I disorder. *Human Brain Mapping*, *37*(1), 122–134.

Collin, G., Scholtens, L. H., Kahn, R. S., Hillegers, M. H., & van den Heuvel, M. P. (2017). Affected anatomical rich club and structural–functional coupling in young offspring of schizophrenia and bipolar disorder patients. *Biological psychiatry*, *82*(10), 746-755.

D'Esposito, M., Deouell, L. Y., & Gazzaley, A. (2003). Alterations in the BOLD fMRI signal with ageing and disease: a challenge for neuroimaging. *Nature Reviews Neuroscience*, *4*(11), 863–872.

Damme, K. S. F., Young, C. B., & Nusslock, R. (2017). Elevated nucleus accumbens structural connectivity associated with proneness to hypomania: A reward hypersensitivity perspective. *Social Cognitive Affective Neuroscience, 12*(6), 928-936.

Damoiseaux, J. S., & Greicius, M. D. (2009). Greater than the sum of its parts: a review of studies combining structural connectivity and resting-state functional connectivity. *Brain Structure and Function*, *213*(6), 525–533.

Damoiseaux, J. S., Rombouts, S. A. R. B., Barkhof, F., Scheltens, P., Stam, C. J., Smith, S. M., & Beckmann, C. F. (2006). Consistent resting-state networks across healthy subjects. *Proceedings of the National Academy of Sciences*, *103*(37), 13848–13853.

Deco, G., Jirsa, V. K., & McIntosh, A. R. (2011). Emerging concepts for the dynamical organization of resting-state activity in the brain. *Nature Reviews. Neuroscience*, *12*(1), 43–56.

Deco, G., Ponce-Alvarez, A., Mantini, D., Romani, G. L., Hagmann, P., & Corbetta, M. (2013).

Resting-State Functional Connectivity Emerges from Structurally and Dynamically Shaped Slow Linear Fluctuations. *The Journal of Neuroscience*, *33*(27), 11239–11252.

Dennis, E. L., Jahanshad, N., Toga, A. W., McMahon, K. L., De Zubicaray, G. I., Martin, N. G., & Thompson, P. M. (2012). Test-retest reliability of graph theory measures of structural brain connectivity. *International Conference on Medical Image Computing and Computer-Assisted Intervention*, Springer: Berlin, 305-312.

Elliott, R., Dolan, R. J., & Frith, C. D. (2000). Dissociable functions in the medial and lateral orbitofrontal cortex: evidence from human neuroimaging studies. *Cerebral cortex*, *10*(3), 308-317.

Endicott, J., & Spitzer, R. L. (1978). A diagnostic interview: the schedule for affective disorders and schizophrenia. *Archives of General Psychiatry*, *35*(7), 837–844.

Fischl, B. (2012). FreeSurfer. *Neuroimage*, *62*(2), 774–781.

Fischl, B., Salat, D. H., Busa, E., Albert, M., Dieterich, M., Haselgrove, C., & Dale, A. M. (2002). Whole brain segmentation: automated labeling of neuroanatomical structures in the human brain. *Neuron*, *33*, 341–355.

Forde, N. J., O'Donoghue, S., Scanlon, C., Emsell, L., Chaddock, C., Leemans, A., & McDonald, C. (2015). Structural brain network analysis in families multiply affected with bipolar I disorder. *Psychiatry Research: Neuroimaging*, *234*(1), 44–51.

Fornito, A., & Bullmore, E. T. (2015). Connectomics: A new paradigm for understanding brain disease. *European Neuropsychopharmacology*, *25*(5), 733–748.

Fornito, A., Zalesky, A., & Breakspear, M. (2013). Graph analysis of the human connectome: Promise, progress, and pitfalls. *NeuroImage*, *80*, 426–444.

Fox, M. D., & Raichle, M. E. (2007). Spontaneous fluctuations in brain activity observed with functional magnetic resonance imaging. *Nature Reviews. Neuroscience*, *8*(9), 700–711.

GadElkarim, J. J., Ajilore, O., Schonfeld, D., Zhan, L., Thompson, P. M., Feusner, J. D., & Leow, A. D. (2014). Investigating brain community structure abnormalities in bipolar disorder using path length associated community estimation. *Human Brain Mapping*, *35*(5), 2253–2264.

Greicius, M. D., Supekar, K., Menon, V., & Dougherty, R. F. (2009). Resting-state functional connectivity reflects structural connectivity in the default mode network. *Cerebral Cortex (New York, N.Y.: 1991)*, *19*(1), 72–78.

Gross, J. J. (2002). Emotion regulation: Affective, cognitive, and social consequences. *Psychophysiology*, *39*, 281–291.

Goodwin, F. K., and Jamison, K. R. (2007) Manic-depressive illness: bipolar disorders and recurrent depression. Oxford University Press.

Haber, S. N., & Behrens, T. E. J. (2014). The Neural Network Underlying Incentive-Based Learning: Implications for Interpreting Circuit Disruptions in Psychiatric Disorders. *Neuron*, *83*(5), 1019–1039.

Haber, S. N., & Knutson, B. (2010). The reward circuit: linking primate anatomy and human imaging. *Neuropsychopharmacology*, *35*(1), 4–26.

Howard, J. D., & Kahnt, T. (2017). Identity-specific reward representations in orbitofrontal cortex are modulated by selective devaluation. *The Journal of Neuroscience, 37*(10), 2627-2638.

Johnson, S. L., Edge, M. D., Holmes, M. K., & Carver, C. S. (2012). The Behavioral Activation

System and Mania. *Annual Review of Clinical Psychology, 8*(*8*), 243–267.

Kochman, F. J., Hantouche, E. G., Ferrari, P., Lancrenon, S., Bayart, D., & Akiskal, H. S. (2005). Cyclothymic temperament as a prospective predictor of bipolarity and suicidality in children and adolescents with major depressive disorder. *Journal Affective Disorder*, *85*(1–2), 181–189.

Kringelbach, M. L., & Berridge, K. C. (2009). Towards a functional neuroanatomy of pleasure and happiness. *Trends in Cognitive Science*, *13*(11), 479–487.

Kringelbach, M. L. (2005). The human orbitofrontal cortex: linking reward to hedonic experience. *Nature Reviews Neuroscience*, *6*(9), 691

Kruschwitz, J. D., List, D., Waller, L., Rubinov, M., & Walter, H. (2015). GraphVar: A user-friendly toolbox for comprehensive graph analyses of functional brain connectivity. *Journal of Neuroscience Methods*, *245*, 107-115.

Lebel, C., Walker, L., Leemans, A., Phillips, L., & Beaulieu, C. (2008). Microstructural maturation of the human brain from childhood to adulthood. *Neuroimage*, *40*(3), 1044-1055.

Leow, A., Ajilore, O., Zhan, L., Arienzo, D., GadElkarim, J., Zhang, A., & Altshuler, L. (2013). Impaired Inter-Hemispheric Integration in Bipolar Disorder Revealed with Brain Network Analyses. *Biological Psychiatry*, *73*(2), 183–193.

Logothetis, N. K. (2003). The Underpinnings of the BOLD Functional Magnetic Resonance Imaging Signal. *The Journal of Neuroscience*, *23*(10), 3963 LP-3971.

Manelis, A., Almeida, J. R. C., Stiffler, R., Lockovich, J. C., Aslam, H. A., & Phillips, M. L. (2016). Anticipation-related brain connectivity in bipolar and unipolar depression: a graph

theory approach, *Brain, 139*(9), 2554–2566.

Marchand, W. R., Lee, J. N., Garn, C., Thatcher, J., Gale, P., Kreitschitz, S., & Wood, N. (2011). Aberrant emotional processing in posterior cortical midline structures in bipolar II depression. *Progress in Neuro-Psychopharmacology & Biological Psychiatry*, *35*(7), 1729–1737.

Mayberg, H. S. (1997). Limbic-cortical dysregulation: a proposed model of depression. *The Journal of Neuropsychiatry and Clinical Neurosciences*, *9*(3), 471–481.

Merikangas, K. R., Akiskal, H. S., Angst, J., Greenberg, P. E., Hirschfeld, R. M. A., Petukhova, M., & Kessler, R. C. (2007). Lifetime and 12-Month Prevalence of Bipolar Spectrum Disorder in the National Comorbidity Survey Replication. *Archives of General Psychiatry*, *64*(5), 543–552.

Meyer, B., Beevers, C. G., & Johnson, S. L. (2004). Goal Appraisals and Vulnerability to Bipolar Disorder: A Personal Projects Analysis. *Cognitive Therapy and Research*, *28*(2), 173–182.

Meyer, B., Johnson, S. L., & Winters, R. (2001). Responsiveness to threat and incentive in bipolar disorder. Relations of the BIS/BAS scales with symptoms. *23*, 133–143.

Mills, K. L., Goddings, A. L., Herting, M. M., Meuwese, R., Blakemore, S. J., & Crone, E. A. (2016) Structural brain development between childhood and adulthood: Convergence across four longitudinal samples. *Neuroimage, 141*, 273-281.

Mills, K. L., & Tamnes, C. K. (2014) Methods and considerations for longitudinal structural brain imaging analysis across development. *Developmental cognitive neuroscience, 9*, 172-190.

Murugesan, S., Bouchard, K., Brown, J. A., Hamann, B., Seeley, W. W., Trujillo, A., & Weber, G. H. (2017). Brain modulyzer: Interactive visual analysis of functional brain connectivity. *IEEE/ACM Transactions on Computational Biology and Bioinformatics (TCBB)*, *14*(4), 805-818.

Nusslock, R., & Alloy, L. B. (2017). Reward processing and mood-related symptoms: An RDoC and translational neuroscience perspective. *Journal of Affective Disorders*, *216*, 3–16.

Nusslock, R., Almeida, J. R., Forbes, E. E., Versace, A., Frank, E., Labarbara, E. J., & Phillips, M. L. (2012). Waiting to win: elevated striatal and orbitofrontal cortical activity during reward anticipation in euthymic bipolar disorder adults. *Bipolar Disord*, *14*(3), 249–260.

Nusslock, R., Young, C. B., & Damme, K. S. F. (2014). Elevated reward-related neural activation as a unique biological marker of bipolar disorder: Assessment and treatment implications. *Behaviour Research and Therapy*, *62*, 74-87.

O'Donoghue, S., Kilmartin, L., O'Hora, D., Emsell, L., Langan, C., McInerney, S., & McCarthy, P. (2017). Anatomical integration and rich-club connectivity in euthymic bipolar disorder. *Psychological medicine*, *47*(9), 1609-1623.

Paus, T., Keshavan, M., & Giedd, J. N. (2008) Why do many psychiatric disorders emerge during adolescence? *Nature Reviews Neuroscience*. *9*(12), 947.

Phillips, M. L., Ladouceur, C. D., & Drevets, W. C. (2008). A neural model of voluntary and automatic emotion regulation: implications for understanding the pathophysiology and neurodevelopment of bipolar disorder. *Molecular Psychiatry*, *13*(9), 829–857.

Poldrack, R. A., Laumann, T. O., Koyejo, O., Gregory, B., Hover, A., Chen, M.-Y., & Mumford, J. A. (2015). Long-term neural and physiological phenotyping of a single human. *Nature*

Communications, *6*, 8885.

Roberts, G., Lord, A., Frankland, A., Wright, A., Lau, P., Levy, F., & Breakspear, M. (2017). Functional Dysconnection of the Inferior Frontal Gyrus in Young People with Bipolar Disorder or at Genetic High Risk. *Biological Psychiatry*, *81*(8), 718–727.

Rubinov, M., & Sporns, O. (2010). Complex network measures of brain connectivity: Uses and interpretations. *NeuroImage*, *52*(3), 1059–1069.

Sacchet, M. D., Ho, T. C., Connolly, C. G., Tymofiyeva, O., Lewinn, K. Z., Han, L. K., & Yang, T. T. (2016). Large-Scale Hypoconnectivity Between Resting-State Functional Networks in Unmedicated Adolescent Major Depressive Disorder. *Neuropsychopharmacology*, *41*(12), 2951–2960.

Saunders, E. F., Fernandez-Mendoza, J., Kamali, M., Assari, S., & McInnis, M. G. (2015). The effect of poor sleep quality on mood outcome differs between men and women: a longitudinal study of bipolar disorder. *Journal of affective disorders*, *180*, 90-96.

Schultz, W. (2000). Multiple reward signals in the brain. *Nat Rev Neurosci*, *1*(3), 199–207.

Seehaus, A., Roebroeck, A., Bastiani, M., Fonseca, L., Bratzke, H., Lori, N., & Galuske, R. (2015). Histological validation of high-resolution DTI in human post mortem tissue. *Frontiers in Neuroanatomy*, *9*, 98.

Shehzad, Z., Kelly, A. M. C., Reiss, P. T., Gee, D. G., Gotimer, K., Uddin, L. Q., & Milham, M. P. (2009). The Resting Brain: Unconstrained yet Reliable. *Cerebral Cortex*, *19*(10), 2209–2229.

Spielberg, J. M., Beall, E. B., Hulvershorn, L. A., Altinay, M., Karne, H., & Anand, A. (2016). Resting State Brain Network Disturbances Related to Hypomania and Depression in

Medication-Free Bipolar Disorder. *Neuropsychopharmacology*, *41*(13), 3016–3024.

Sporns, O. (2011). The human connectome: A complex network, *1224*, 109–125.

Strakowski, S. M., Adler, C. M., Almeida, J., Altshuler, L. L., Blumberg, H. P., Chang, K. D., DelBello, M. P., Frangou, S., McIntosh, A., Phillips, M. L., Sussman, J. E., & Townsend, J. D. (2012). The functional neuroanatomy of bipolar disorder: a consensus model. *Bipolar Disorders*, *14*(4), 313–325.

Torrubia, R., Ávila, C., Moltó, J., & Caseras, X. (2001). The Sensitivity to Punishment and Sensitivity to Reward Questionnaire (SPSRQ) as a measure of Gray's anxiety and impulsivity dimensions. *Personality and Individual Differences*, *31*(6), 837–862.

Urosevic, S., Abramson, L. Y., Harmon-Jones, E., & Alloy, L. B. (2008). Dysregulation of the behavioral approach system (BAS) in bipolar spectrum disorders: review of theory and evidence. *Clinical Psychological Review*, *28*(7), 1188–1205.

van den Heuvel, M. P., Sporns, O., Collin, G., Scheewe, T., Mandl, R. C., Cahn, W., & Kahn, R. S. (2013). Abnormal rich club organization and functional brain dynamics in schizophrenia. *JAMA psychiatry*, *70*(8), 783-792.

Vollmar, C., O'Muircheartaigh, J., Barker, G. J., Symms, M. R., Thompson, P., Kumari, V., & Koepp, M. J. (2010). Identical, but not the same: Intra-site and inter-site reproducibility of fractional anisotropy measures on two 3.0 T scanners. *NeuroImage*, *51*(4), 1384–1394.

Wang, Y., Deng, F., Jia, Y., Wang, J., Zhong, S., Huang, H., & Huang, R. (2018). Disrupted rich club organization and structural brain connectome in unmedicated bipolar disorder. *Psychological medicine*, 1-9.

Whitton, A. E., Treadway, M. T., & Pizzagalli, D. A. (2015). Reward processing dysfunction in

major depression, bipolar disorder and schizophrenia. *Current Opinion in Psychiatry*, *28*(1), 7–12.

Zhang, J., Wang, J., Wu, Q., Kuang, W., Huang, X., & Gong, Q. (2011). Disrupted Brain Connectivity Networks in Drug-Naive, *Biological Psychiatry, 70*(19), 334-342.

Zilles, K., Armstrong, E., Schleicher, A., & Kretschmann, H. J. (1988). The human pattern of gyrification in the cerebral cortex. *Anatomy and Embryology*, *179*(2), 173–179.

Table 1. Demographics Across Groups

MRI Study Sample	Low-Risk *M(SD)*	High-Risk *M(SD)*	BSD *M(SD)*	Total *M(SD)*	Group Comparison	*p-value*
Age	21.11(1.91)	20.55(1.91)	20.56(1.91)	20.74 (1.93)	$F(129,2)=1.77$	0.19
Sex	22 F/22 M	29 F/24 M	18 F/24 M	69 F/62 M	$\chi^2= .22$	0.89
Handedness	14.23 (1.91)	14.63 (2.59)	14.03 (1.56)	14.15 (2.11)	$F(129,2)=0.17$	0.68

M = mean, SD = Standard Deviation

Table 2. Reward Sensitivity Across Groups

Reward Sensitivity	Low-Risk *M(SD)*	High-Risk *M(SD)*	BSD *M(SD)*	Total *M(SD)*	Group Comparison	*p-value*
BAS Total	37.83 (1.08)	45.55(2.83)	46.03 (3.54)	43.13 (4.56)	*F*(131,2)= 135.5	<0.0001
					Post-hoc	
				BSD vs High-Risk	t(87,2)= 0.66	0.5
				BSD vs Low-Risk*	t(78,2)= 13.03	<0.0001
				High-Risk vs Low-Risk*	t(97,2)= 17.94	<0.0001
				Total *M(SD)*	Group Comparison	*p-value*
Sensitivity to Reward Subscale	11.05 (1.48)	18.00 (3.40)	17.21 (2.93)	15.54 (4.17)	*F*(131,2)= 66.76	<0.0001
					Post-hoc	
				BSD vs High-Risk	t(87,2)= -1.14	0.26
				BSD vs Low-Risk*	t(78,2)= 11.09	<0.0001
				High-Risk vs Low-Risk*	t(97,2)= 12.97	<0.0001

BSD = Bipolar Spectrum Disorders, M = mean, SD = Standard Deviation

Table 3. Diagnostic Clinical Group Comparison: Counts for each group on the presence or absence of the diagnosis or medication.

Diagnosis	Low-Risk	High-Risk	BSD	Total	χ^2	*p-value*
Any Diagnoses (non-BSD)	26	40	20	86	3.81	0.14
Subthreshold Depression	8	6	1	15	4.39	0.11
Unipolar Depression*	13	26	0	39	23.84	<.0001*
Any Depression*	21	32	1	54	29.36	<.0001*
Anxiety Disorder	9	18	13	40	3.35	0.19
PTSD	2	3	0	5	1.9	0.38
ADHD*	0	6	1	7	6.62	0.03
Substance Use Disorder	9	8	10	27	2.596	0.27
Eating Disorder	1	2	3	6	2.01	0.36
OCD	0	2	2	4	2.39	0.30
Medication	6	6	4	16	0.165	0.76

BSD = Bipolar Spectrum Disorders

Table 4. Main Effect of Group on Global Metrics by Network Definition

Structural Connectivity	Clustering Coefficient		Path Length	
Network Definition	*F-value*	*p-value*	*F-value*	*p-value*
Whole Brain Network	0.10	0.93	0.15	0.86
Emotion Generation/Regulation Subnetwork	0.10	0.91	1.31	0.94
Reward Subnetwork	1.07	0.35	3.24	0.03

Functional Connectivity	Clustering Coefficient		Path Length	
Network Definition	*F-value*	*p-value*	*F-value*	*p-value*
Whole Brain Network	0.17	0.89	0.17	0.85
Emotion Generation/Regulation Subnetwork	0.13	0.88	1.36	0.26
Reward Subnetwork	0.48	0.62	0.50	0.61

Table 5. Main Effect of High Risk Group Nodal Graph Metric in Theoretical Internetwork Hub in Structural Connectivity Analyses

Structural Connectivity	Clustering Coefficient		Path Length	
	F-value	*p-value*	*F-value*	*p-value*
Whole Brain Network				
lOFC	0.97	0.38	0.45	0.64
mOFC	0.28	0.76	0.35	0.78
VS	0.91	0.41	1.09	0.34
Amygdala	0.27	0.76	0.59	0.56
Emotion Generation/Regulation Subnetwork				
lOFC	1.78	0.17	2.49	0.09
mOFC	0.11	0.89	1.02	0.36
VS	0.98	0.38	0.49	0.62
Amygdala	0.4	0.35	2.95	0.06
Reward Subnetwork				
lOFC	1.14	0.32	0.21	0.81
mOFC	2.62	0.07*	0.88	0.42
VS	0.53	0.59**	0.11	0.90
Amygdala	0.28	0.76	0.12	0.89

lOFC = lateral orbitofrontal cortex, mOFC = medial orbitofrontal cortex, VS = nucleus accumbens

**There was a trend group by hemisphere interaction on clustering coefficient in the mOFC, $F(2,120)=4.06$, $p=.020$, that did not meet the correction for multiple comparison*

***There was a significant sex by group by hemisphere interaction on clustering coefficient in the VS, $F(2,120)=5.00$, $p=.008$, see Figure 5*

Table 6. Main Effect of High Risk Group Nodal Graph Metric in Theoretical Internetwork Hub in Functional Connectivity Analyses

Functional Connectivity	Clustering Coefficient		Path Length	
	F-value	*p-value*	*F-value*	*p-value*
Whole Brain Network				
lOFC	4.26	0.02*	0.08	0.92
mOFC	0.35	0.70	1.64	0.20
VS	1.54	0.22	1.33	0.27
Amygdala	0.41	0.66	0.23	0.79
Emotion Generation/Regulation Subnetwork				
lOFC	1.91	0.15	2.55	0.08
mOFC	0.07	0.93	1.05	0.35
VS	0.46	0.63	1.1	0.34
Amygdala	0.41	0.67	2.68	0.06
Reward Subnetwork				
lOFC	0.8	0.45	0.65	0.53
mOFC	2.5	0.09	1.20	0.20
VS	0.12	0.72	0.50	0.61
Amygdala	0.44	0.64	1.5	0.23

*lOFC – lateral orbitofrontal cortex, mOFC – medial orbitofrontal cortex, VS – nucleus accumbens, *Trend main effect of group did not meet the correction for multiple comparison*

Table 7. Sex by Group by Hemisphere Interaction in the Medial Orbitofrontal Cortex Theoretical Network Hub in Reward Subnetwork

Group	Hemisphere	*M*	*SEM*	95% Confidence Interval
Male				
Low-Risk Group	Left	0.31	0.042	0.226-0.393
	Right	0.152	0.043	0.068-0.237
High-Risk Group	Left	0.153	0.039	0.077-0.233
	Right	0.197	0.04	0.118-0.276
BSD Group	Left	0.131	0.047	0.079-0.265
	Right	0.249	0.048	0.151-0.345
Female				
Low-Risk Group	Left	0.116	0.043	0.310-0.202
	Right	0.153	0.044	0.060-0.240
High-Risk Group	Left	0.127	0.036	0.057-0.189
	Right	0.126	0.036	0.055-0.198
BSD Group	Left	0.172	0.047	0.079-0.265
	Right	0.122	0.048	0.226-0.216

BSD = Bipolar Spectrum Disorders, M = mean, SEM = Standard Error of the Mean

Figure 1. Structural Path Length in the Ventrolateral Prefrontal Cortex (dlPFC) by Group in the Emotion Generation/Regulation Subnetwork: A. Shows Group Connectivity of vlPFC in the Emotion Generation/Regulation Subnetworks, B. Significant Group Average Path Length in the vlPFC (p=.004)

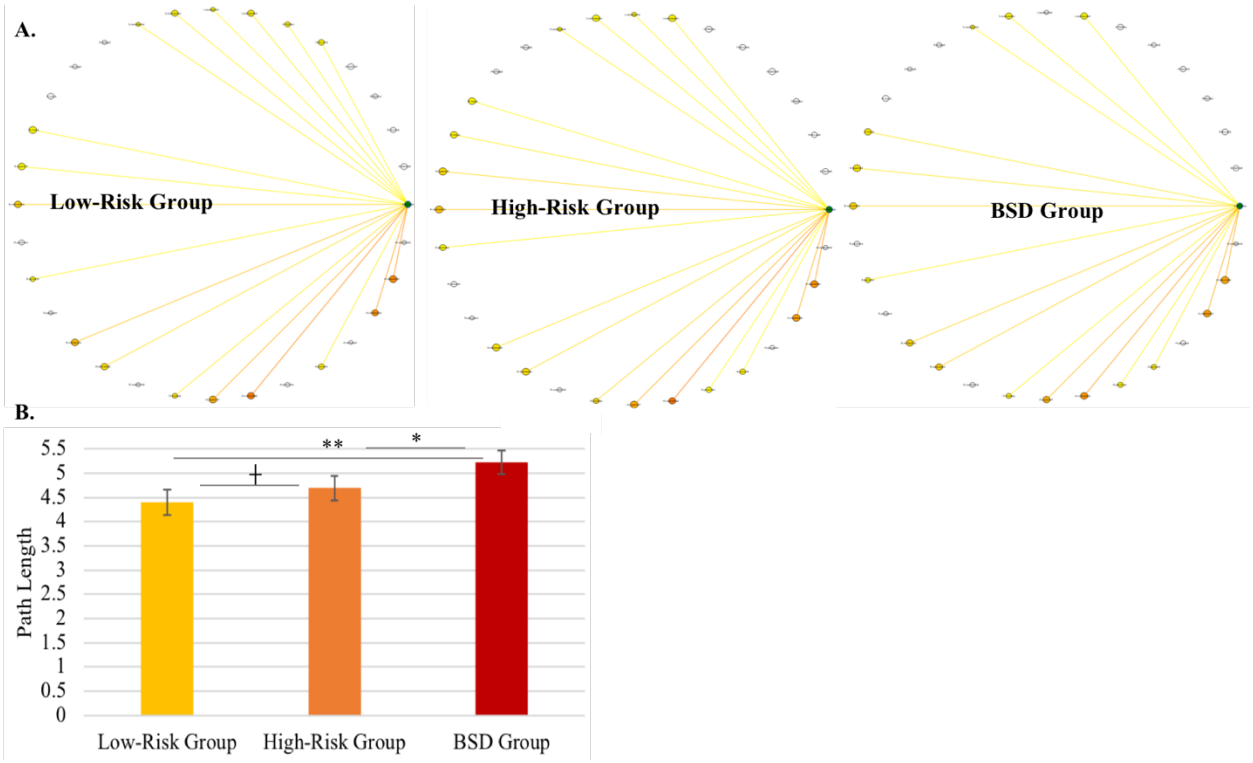

vlPFC - Ventrolateral Prefrontal Cortex, BSD – Bipolar Spectrum Disorders - BSD

** p=.001, * p=.05, + p=.06

Figure 2. Structural Path Length in the Left Amygdala by Group in the Emotion Generation/Regulation Subnetwork: A. Shows Group Connectivity of Left Amygdala in the Emotion Generation/Regulation Subnetworks, B. Significant Group Average Path Length in the Left Amygdala (*p*=.02)

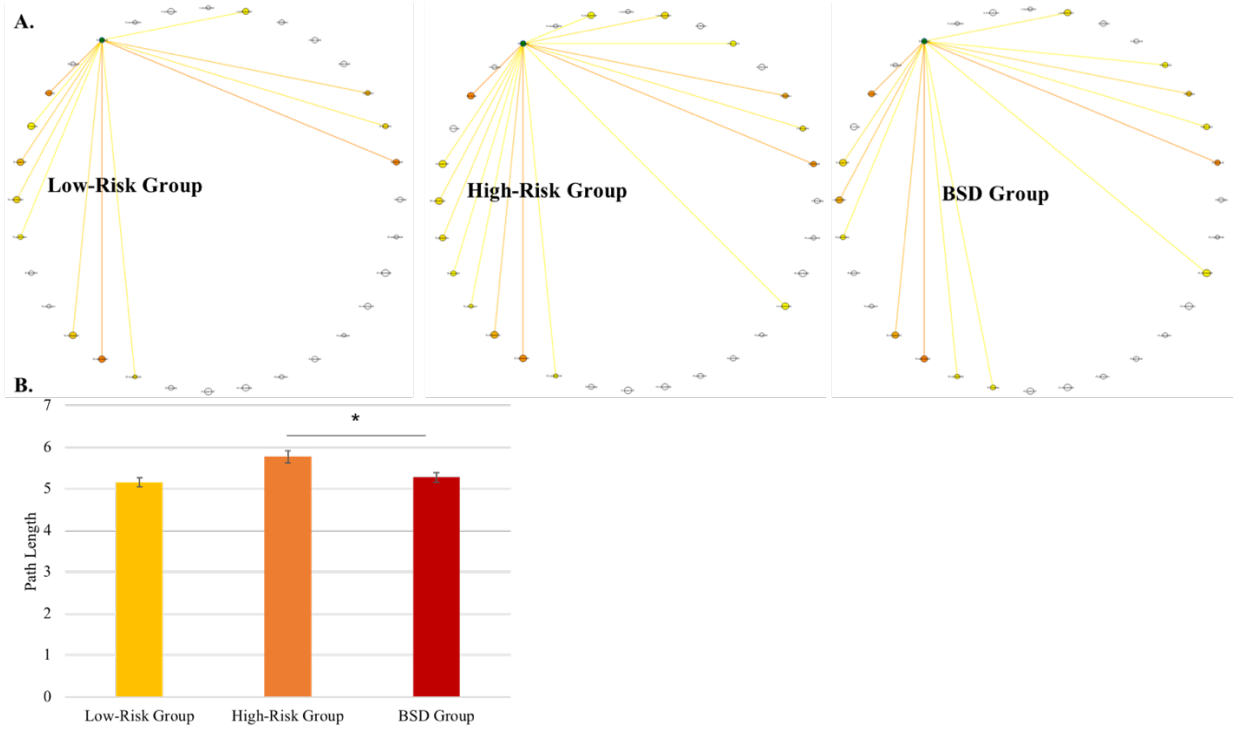

BSD – Bipolar Spectrum Disorders – BSD, * *p*=.001

Figure 3. Structural Clustering Coefficient in the Ventral Striatum by Group and Sex in the Reward Subnetwork (p=.008)

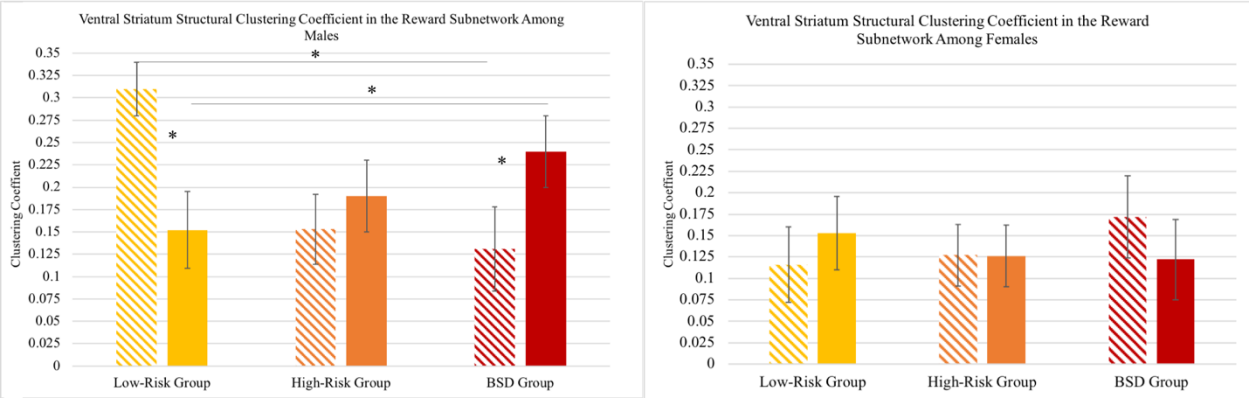

BSD – Bipolar Spectrum Disorders – BSD; * p<.05

Figure 4. Functional Clustering Coefficient in the Dorsal Anterior Cingulate Cortex (dlPFC) by Group in the Emotion Generation/Regulation Subnetwork: A. Shows Group Connectivity of dlPFC in the Emotion Generation/Regulation Subnetworks, B. Significant Group Average Path Length in the dlPFC (p=.001)

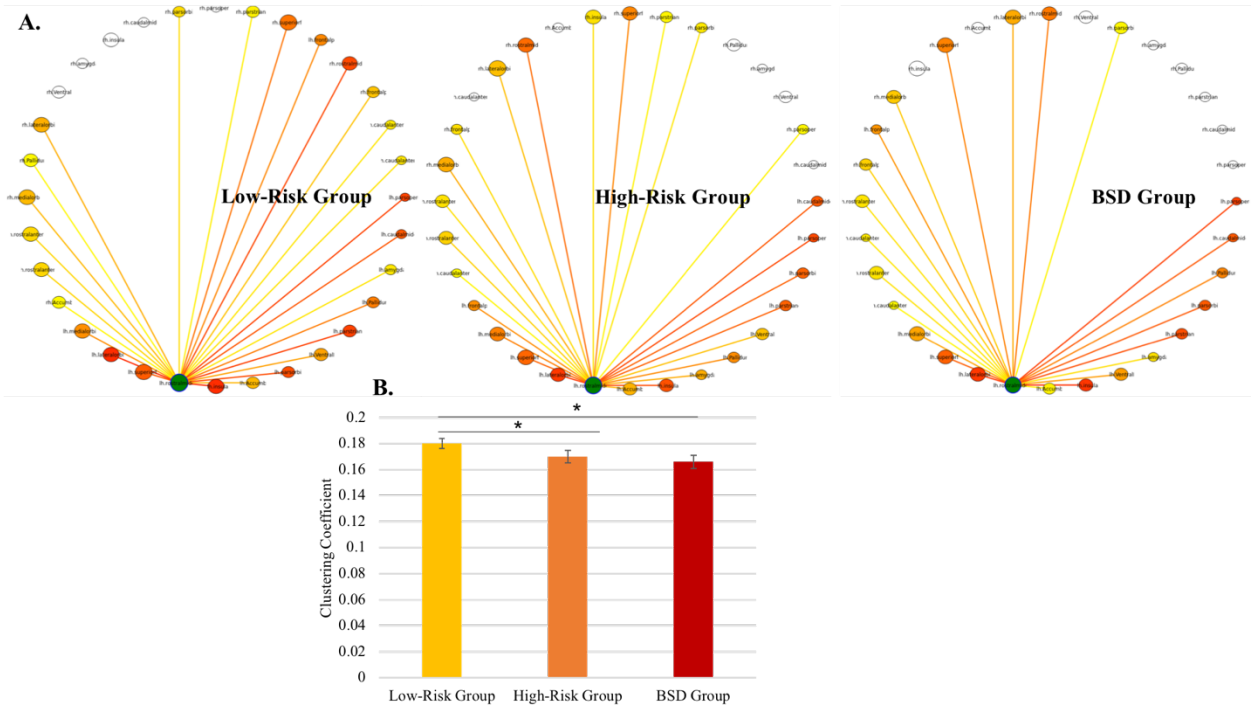

BSD – Bipolar Spectrum Disorders – BSD; * p<.003

Figure 5. Functional Path Length in the Dorsal Anterior Cingulate Cortex (dACC) by Group in the Emotion Generation/Regulation Subnetwork: A. Shows Group Connectivity of dACC in the Emotion Generation/Regulation Subnetworks, B. Significant Group Average Path Length in the dACC (*p*=.001)

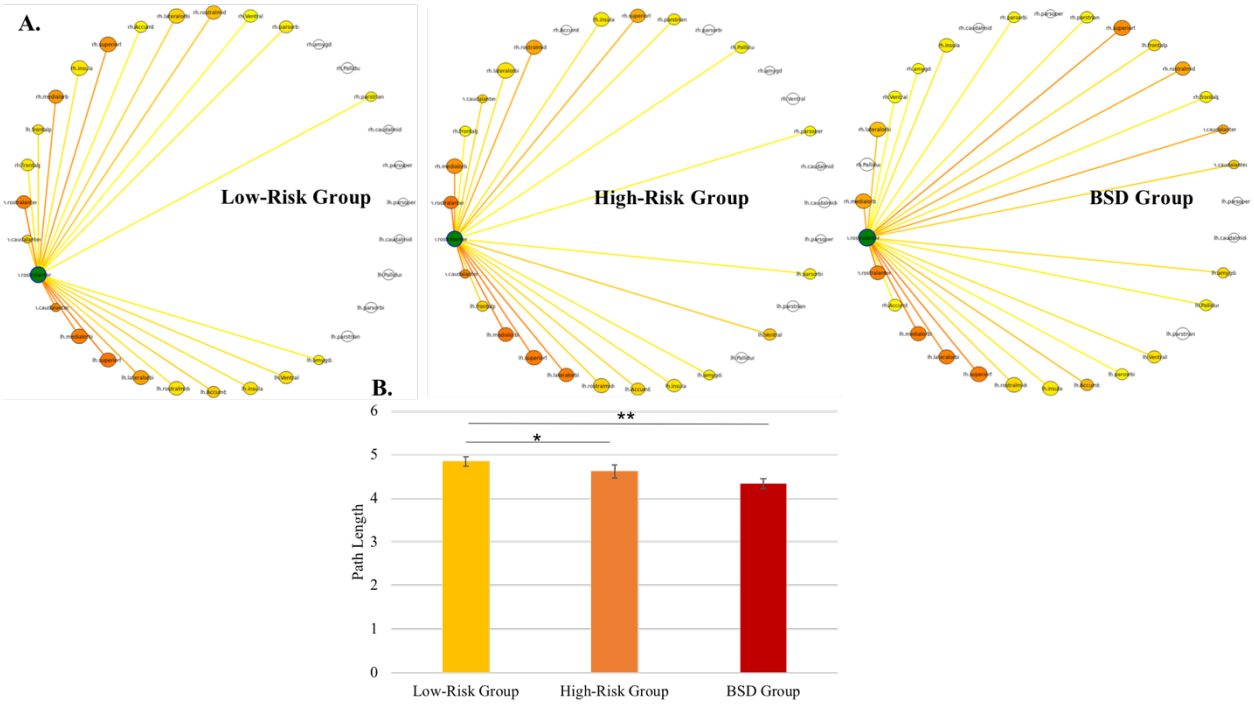

dACC - Dorsal Anterior Cingulate Cortex, BSD – Bipolar Spectrum Disorders – BSD

** *p*=.005 * *p*=.05